AGU100 ADVANCING EARTH AND SPACE SCIENCE

JGR

Journal of Geophysical Research: Atmospheres

RESEARCH ARTICLE

10.1029/2017JD028074

Special Section:
Studies of Emissions and Atmospheric Composition, Clouds and Climate Coupling by Regional Surveys, 2013 (SEAC4RS)

Key Points:
- Relationship between sub-2.5 μm particulate matter and AOD in the SEUS is observed to vary significantly both temporally and spatially
- Extensive southeastern United States sub-2.5 μm particulate matter chemical and optical characterization are provided for the time period of the SEAC^{4}RS campaign and compared to that available two decades prior to the campaign
- Strong intersite correlations among the geographically similar sites in both the chemical constituents and total $PM_{2.5}$ mass result in spatial interpolation among ground stations a more reliable predictor of $PM_{2.5}$ than site-specific AOD measurements

Supporting Information:
- Supporting Information S1

Correspondence to:
K. C. Kaku,
katie.kaku.ctr@nrlmry.navy.mil

Citation:
Kaku, K. C., Reid, J. S., Hand, J. L., Edgerton, E. S., Holben, B. N., Zhang, J., & Holz, R. E. (2018). Assessing the challenges of surface-level aerosol mass estimates from remote sensing during the SEAC^{4}RS and SEARCH campaigns: Baseline surface observations and remote sensing in the southeastern United States. *Journal of Geophysical Research: Atmospheres*, *123*, 7530–7562. https://doi.org/10.1029/2017JD028074

Received 16 NOV 2017
Accepted 15 JUN 2018
Accepted article online 25 JUN 2018
Published online 25 JUL 2018

©2018. The Authors.
This is an open access article under the terms of the Creative Commons Attribution-NonCommercial-NoDerivs License, which permits use and distribution in any medium, provided the original work is properly cited, the use is non-commercial and no modifications or adaptations are made.
This article has been contributed to by US Government employees and their work is in the public domain in the USA.

Assessing the Challenges of Surface-Level Aerosol Mass Estimates From Remote Sensing During the SEAC^{4}RS and SEARCH Campaigns: Baseline Surface Observations and Remote Sensing in the Southeastern United States

K. C. Kaku[1], J. S. Reid[2], J. L. Hand[3], E. S. Edgerton[4], B. N. Holben[5], J. Zhang[6], and R. E. Holz[7]

[1]CSRA, Monterey, CA, USA, [2]Naval Research Laboratory, Monterey, CA, USA, [3]Cooperative Institute for Research in the Atmosphere, Colorado State University, Fort Collins, CO, USA, [4]Atmospheric Research and Analysis, Inc., Cary, NC, USA, [5]NASA, Greenbelt, MD, USA, [6]Department of Atmospheric Sciences, University of North Dakota, Grand Forks, ND, USA, [7]CIMSS, University of Wisconsin, Madison, WI, USA

Abstract The Studies of Emissions and Atmospheric Composition, Clouds and Climate Coupling by Regional Surveys (SEAC^{4}RS) campaign conducted in the southeast United States (SEUS) during the summer of 2013 provided a singular opportunity to study local aerosol chemistry and investigate aerosol radiative properties and $PM_{2.5}$ relationships, focusing on the complexities involved in simplifying the relationship into a linear regression. We utilize three Southeastern Aerosol Research and Characterization network sites and one Environmental Protection Agency Chemical Speciation Network station that afforded simultaneous Aerosol Robotic Network (AERONET) aerosol optical depth (AOD) and aerosol mass, chemistry, and light scattering monitoring. Prediction of AERONET AOD using linear regression of daily-mean $PM_{2.5}$ during the SEAC^{4}RS campaign yielded r^2 of 0.36–0.53 and highly variable slopes across four sites. There were further reductions in $PM_{2.5}$ predictive skill using Moderate Resolution Imaging Spectroradiometer (MODIS) and Multi-angle Imaging SpetroRadiometer (MISR) AOD data, which have shorter correlation lengths and times relative to surface $PM_{2.5}$. Long-term trends in aerosol chemistry and optical properties in the SEUS are also investigated and compared to SEAC^{4}RS period data, establishing that the SEUS experienced significant reduction in aerosol mass, corresponding with changes in both aerosol chemistry and optical properties. These changes have substantial impact on the $PM_{2.5}$-AOD linear regression relationship and reinforce the need for long-term aerosol observation stations in addition to concentrated field campaigns.

1. Introduction

The influence of surface-level particulate matter with a diameter below 2.5 μm ($PM_{2.5}$) to human health and visual air quality has long been recognized (e.g., Brown et al., 1950; Englert, 2004) and was formalized in U.S. environmental regulation by the establishment of the Clean Air Act in 1970. Surface level concentrations are monitored routinely within the United States by more than 4,000 stations operated by state environmental agencies as required by the Environmental Protection Agency (EPA) and the Clean Air Act (https://www3.epa.gov/airdata/ad_basic.html). Additionally, the World Health Organization reports $PM_{2.5}$ data collected by almost 1,600 cities in 91 countries (http://www.who.int/phe/health_topics/outdoorair/databases/cities/en/). Despite this extensive network, global $PM_{2.5}$ concentration data are collected with inconsistent protocols and are prone to large spatial and temporal gaps. Continuous global monitoring of air quality is desired by many health, environmental, climate, and operational organizations.

There has been continued optimism in the scientific community that satellite systems can aid in global monitoring of surface aerosol properties such as $PM_{2.5}$ for air quality applications (e.g., Al-Saadi et al., 2005; Hoff & Christopher, 2009). Scientists have tried to correlate commonly retrieved aerosol optical depth (AOD) from satellite sensors to surface $PM_{2.5}$ (e.g., Engel-Cox et al., 2005; Wang & Christopher, 2003). However, such regressions have mixed results when systematically reviewed over multiple sites and seasons, with coefficients of determination (r^2) rarely above 0.5, and in some cases showed statistically insignificant relationships (e.g., Li et al., 2015; Toth et al., 2014, and references therein). Even when moving to comparisons between lidar backscatter or extinction to $PM_{2.5}$, regression results are only marginally improved at daily levels

(e.g., Reid et al., 2017; Toth et al., 2014). At the same time, assimilation of satellite AOD data into global aerosol models at operational centers is now commonplace (e.g., see Session et al, 2015) and while AOD assimilation clearly improves modeled AOD analyses and forecasts, preliminary assessments of the impact of AOD assimilation on $PM_{2.5}$ forecasting are also quite mixed (e.g., Buchard et al., 2016; McHenry et al., 2015; Reid et al., 2017; Schwartz et al., 2012). This is not to say satellite data have no value, but care and consideration of satellite capabilities should be a priority. Tracking large plumes or major dust events is quite easy. Determining baseline surface concentrations and minor to moderate variations in $PM_{2.5}$ from optical measurement less so (e.g., Reid et al., 2017).

The core problem of reconciling remotely sensed AOD or other aerosol parameters such as aerosol backscatter or extinction to $PM_{2.5}$ lies within variability in $PM_{2.5}$ vertical distribution as well as a number of free intensive parameters including particle mass extinction efficiency, and hygroscopic growth characteristics. These are all well-known sensitivities that have been examined in countless local and column closure studies performed in the field (e.g., Ford & Heald, 2013; Li et al., 2015; Quinn & Coffman, 1998; Ross et al., 1998; Schmid et al., 2000; Shinozuka et al., 2015; Wagner et al., 2015; Wang & Christopher, 2003; Ziemba et al., 2013), and alternatives to linear regressions have been proposed (e.g., Loría-Salazar et al., 2017). Extinction efficiencies and hygroscopicity are in turn nonlinearly dependent on a host of environmental, meteorological, chemical, and microphysical variables. The complex relationship between surface aerosol and AOD is further complicated by the fact that the most commonly monitored parameter, $PM_{2.5,}$ is an air quality monitoring benchmark spanning both the fine mode (FM) and a fraction of the coarse mode. Even relatively small amounts of dust or sea salt may skew the interpretation of $PM_{2.5}$ values (e.g., Atwood et al., 2013). At the same time fundamental AOD, lidar, and $PM_{2.5}$ data quality and sampling frequency are also of concern (Drury et al., 2010; Hyer et al., 2011; Toth et al., 2014; Zhang et al., 2008), as are measurements and model errors in the vertical profile of $PM_{2.5}$, chemistry, extinction, and relative humidity. Comparison of airborne to ground-based measurements are equally problematic. Aerosol samplers are mere meters above the ground in a surface layer that can be decoupled from the rest of planetary boundary layer (PBL; Reid et al., 2017), especially at night.

The problems associated with closure studies of aerosol physical, chemical, and radiative properties in Earth observing and modeling systems are long-standing. However, headway is afforded the community through several significant field campaigns conducted in 2013 over the southeast United States (SEUS): the Studies of Emissions and Atmospheric Composition, Clouds and Climate Coupling by Regional Surveys (SEAC^{4}RS; Toon et al., 2016) and National Science Foundation and National Oceanic and Atmospheric Administration (NSF and NOAA)-sponsored Southeast Nexus study (SENEX; Wagner et al., 2015), as well as the Southern Oxidant and Aerosol Study (SOAS; Budisulistiorini et al., 2015). With its extensive use of aerosol radiation and chemistry data by aircraft and surface station, SEAC^{4}RS, SENEX, and SOAS provided an outstanding and perhaps singular opportunity to date to regionally bridge aerosol radiative and $PM_{2.5}$ properties when placed in the context of long term sampling. Based on available field data, uncertainties in Earth system data sets can be assessed. Fundamental questions on the variability and covariability of aerosol intensive and extensive parameters can be examined. From such examination, we can assess the scales at which aerosol mass, chemistry, and optical properties fundamentally correlate. Most importantly, analyses benchmarks can be developed for gauging agreement between remote sensing data and modeling systems.

As part of SEAC^{4}RS, Aerosol Robotic Network (AERONET) Sun photometers were placed throughout the SEUS (Holben et al., 1998; Toon et al., 2016). These deployments were often in association with air quality sites, such as at Interagency Monitoring of Protected Visual Environments (IMPROVE) stations (Malm et al., 1994). Of significant note, Sun photometers were established at three South Eastern Aerosol Research and Characterization (SEARCH; Hansen et al., 2003) aerosol sites allowing for simultaneous monitoring of AOD and hourly to daily level surface aerosol chemistry and light scattering (Centreville, AL; Outlying Landing Fields, FL; and Yorkville, GA). As part of SEAC^{4}RS, the University of Alabama, Huntsville (UAH), site employed a Sun photometer and measured basic meteorological parameters and was 5 km from an EPA Chemical Speciation Network (CSN) site (U.S. Environmental Protection Agency, 2004), which afforded hourly $PM_{2.5}$ mass, and aerosol chemistry measurements made once every six days. Also at the UAH site was the addition of a University of Wisconsin (UW) Space Sciences and Engineering Center (SSEC) 532 nm high spectral resolution lidar (HSRL) to the University of Alabama Huntsville (UAH) National Space Sciences Technology Center (NSSTC) Regional Atmospheric Profiling Center for Discovery (RAPCD) lidar facility (UW HSRL), providing

near continuous profiles of aerosol backscatter (Reid et al., 2017). Between the SEARCH and UAH sites, we have the ability to regionally monitor AOD-$PM_{2.5}$ relationships and intensive particle scattering and chemistry properties at daily to hourly sampling all spaced ~250 km apart in a roughly 500 × 250 km domain covering portions of the Florida panhandle, Alabama, and northwest Georgia. This spacing is similar to the *e*-folding area of influence used in global aerosol data assimilation (e.g., Rubin et al., 2017; Zhang et al., 2008).

Recently, Reid et al. (2017) used the UW-HSRL at the UAH site to examine the modes of variability in the aerosol vertical profile over the UAH site. Here we go a step further, reviewing radiative property-$PM_{2.5}$ relationships in the neighboring region at SEARCH and CSN sites fitted with AERONET stations for the SEAC^{4}RS mission. We pose the questions: What were the baseline surface $PM_{2.5}$ properties in the core SEUS region? Are there correlations between $PM_{2.5}$, intensive aerosol properties, and AOD at and between sites? Are AOD data from AERONET or satellite providing information in addition to what can be learned by the ground network? Are there correlations between intensive parameters to help constrain the system, such as between the relative organic/inorganic speciation and mass scattering efficiency? How do the aerosol properties measured in 2013 compare to other years? Do these sites capture the overall downward trend in regional pollution? Investigation of this baseline data coupled with the aerosol vertical profile at UAH provided by Reid et al. (2017) sets the stage for more detailed inquiry.

Results for this paper are provided in three parts. First, to set a regional baseline, we will begin with an overview of the aerosol environment at the SEARCH and UAH sites for June–October 2013 including correlations of key measures of aerosol mass and AOD. Notable is a rapid shift in summer to fall aerosol regimes. Next, this work leads into analysis of how the SEAC^{4}RS data fit into the seasonal variations and long-term trends and explore the variability and dependencies of intensive aerosol properties such as mass scattering efficiency, and hygroscopicity as well as relative humidity at the surface. Finally, we explore intersite correlations and how that can be used to improve predictions.

2. Methods and Study Data

Satellite-$PM_{2.5}$ studies are often relatively straightforward with current usage often assuming that AOD measurements combined with model output of simplistic aerosol chemistry are sufficient to predict ground-level $PM_{2.5}$ mass. The AOD retrievals at 550 nm from the Moderate Resolution Imaging Spectroradiometer (MODIS) sensors on the Terra and Aqua satellites are used to provide near global coverage (e.g., Gupta et al., 2006; Kaufman et al., 2000) although other narrower swath sensors such as Multi-angle Imaging SpetroRadiometer (MISR) have also been used (e.g., Kahn et al., 2007; Van Donkelaar et al., 2010). The AOD products are either directly regressed onto a metric such as $PM_{2.5}$ or PM_{10} (Wang & Christopher, 2003), or are applied to vertical distribution using an a priori assumed or model vertical profile (e.g., Liu et al., 2005). When ingested in a data assimilation framework, functionally the vertical profile is often uniformly scaled to match the AOD observation (e.g., Rubin et al., 2017; Zhang et al., 2008). Even pure empirical machine learning based on the input AOD, $PM_{2.5}$, and a host of meteorological parameters is becoming commonplace (e.g., Lary et al., 2009). In the most straightforward technique, such as in the Navy Aerosol Analysis and Prediction System (NAAPS; Lynch et al., 2016), extinction is calculated in a bulk fashion as simply the dry aerosol mass concentrations ($c_{m,\ \mathrm{aero,\ dry}}$), a dry aerosol mass extinction efficiency (α_{ext}), and a factor that describes the interaction of aerosol particles with atmospheric water content, referred to as aerosol hygroscopicity at a given relative humidity, *f* (RH). These are formed in bulk through the linear combination of individual mass species carried in the model (e.g., sea salt, dust, and biomass burning smoke). The vertical integral of the aerosol extinction coefficient yields AOD over height *z* from the surface to the top of the atmosphere (TOA):

$$\mathrm{AOD} = \int_{\mathrm{surface}}^{z_{\mathrm{TOA}}} c_m(z)_{\mathrm{aero,dry}} * \alpha_{\mathrm{ext}}(z) * f(\mathrm{RH}, z)\,dz \tag{1}$$

where *f* (RH,*z*) is the ratio of aerosol scattering coefficients measured at a wet RH (RH_{wet}) and dry RH (RH_{dry}) and can be described using the hygroscopicity parameter, γ (Gassó et al., 2000):

$$f(\mathrm{RH}) = \left(\frac{1 - \frac{\mathrm{RH_{wet}}}{100}}{1 - \frac{\mathrm{RH_{dry}}}{100}}\right)^{-\gamma} \tag{2}$$

Inferring c_m at the surface (or any level) requires error propagation across the AOD observation, the vertical distribution of α_{ext}, *f* (RH), and all of their associated species-related dependencies (e.g., RH (*z*)). This is

Table 1
Summary of Site Characteristics and Instrumentation at the CTR, OLF, and YRK SEARCH Sites and the CSN Site Near the UAH Lidar Facility

	Centreville, AL (CTR)	Outlying Landing Fields, FL (OLF)	Yorkville, GA (YRK)	University of Alabama, Huntsville (UAH)
Lat/Long	32.90°N/87.25°W	30.55°N/87.38°W	33.93°N/85.05°W	34.69°N/86.59°W
Elevation	130 m	40 m	390 m	200 m
Site description	Rural, forested	Seldom used landing strips surrounded by suburban forest/grass	Rural forest/agricultural	Suburban
$PM_{2.5}$ continuous	TEOM (mass), Fe reduction/UV-fluorescence (Sulfate), oxidative combustion (total carbon/OC)			TEOM (mass)
$PM_{2.5}$ 24-hr filter	Teflon 48 mm filter, gravimetry analysis, ion chromatography analysis, Quartz 37 mm filter TOR. Filters collected daily.			Teflon 48 mm filter, gravimetry analysis, LC analysis, Quartz 37 mm filter TOR. Filters collected once every six days.
$PM_{2.5}$ extinction	Nephelometer (λ = 530 nm; dry, RH ~ 20%), aethalometer (λ = 565 nm; dry, RH ~ 20%)			N/A
Surf. meteorology	Temperature, pressure, relative humidity			Temperature, pressure, relative humidity

especially true in the context of data assimilation, where not only the local error is important, but the vertical and horizontal propagation of error as well.

For this study data from four rural to suburban core sites, three SEARCH sites and the UAH site were aggregated during the June–October 2013 SEAC^{4}RS and SENEX deployments. Three SEARCH sites afforded simultaneous AERONET AOD measurements, aerosol mass monitoring, aerosol chemistry, light extinction, and ground weather (Table 1): Centreville (CTR)—aptly in the center of Alabama, Outlying Landing Field (OLF)—in the Florida Panhandle, and Yorkville (YRK)—60 km WNW of Atlanta. In addition, the UAH HSRL lidar site included an AERONET Sun photometer, and a CSN site located 5 km away provided continuous mass measurements, and one day in six aerosol filter measurements. Figure 1 shows the locations of the study area including average kriged $PM_{2.5}$ from the complete EPA's FRM network sites during (a) the summer regime of the SEAC^{4}RS data set (1 June to 20 September 2013), and (b) the fall regime (21 September to 31 October 2013), as identified in Reid et al. (2017), and (c) and (d) Terra MODIS AOD (550 nm) over the same time periods, respectively. A National Aeronautics and Space Administration (NASA) Blue Marble map of the SEARCH and CSN sites used is provided in (e). Kriging data are a technique performed on geographical data sets where Gaussian process regression is used to interpolate as it provides prediction of unknown values where the known values are weighted based on spatial dependence (Yu et al., 2011). Finally, to give a sense of scale of a large air quality event in the region without significant outside transport, a Terra MODIS level 2 AOD product for observed during the SEAC^{4}RS mission, 9 September 2013, is provided in (f). Note the high AOD halos surrounding the regions of convective clouds, suggesting high spatial variability of the aerosol mass and/or hygroscopicity on this day with high aerosol loading. A description of SEAC^{4}RS can be found in Toon et al. (2016), with a detailed description of the UAH site in Reid et al. (2017). Thus, here we only provide a brief overview of the instruments used for this work.

2.1. Aerosol Robotic Network Measurements

An overview plot of the locations and monthly mean AODs from Version 2 AERONET stations throughout the summertime 2013 period is provided in Toon et al. (2016). AERONET data can be accessed at https://aeronet.gsfc.nasa.gov/. However, a few details of the data analyzed are provided here. Only Level-2 AERONET data, postcalibrated and screened for cloud contamination, were utilized in this study (Holben et al., 1998; Smirnov et al., 2000). The data analyzed from all AERONET instruments for this study had a 3-min AOD observation protocol invoked. For the purpose of this study, the Level 2-provided hourly and daily means were utilized. For comparison to satellite measurements and model estimates, AERONET AODs at all four sites were converted to a baseline 550 nm total, fine, and coarse mode AOD using the spectral deconvolution algorithm (SDA+), a methodology that uses a polynomial fit of AOD at multiple wavelengths to capture the first and second derivatives of total AOD versus wavelength and can thus be utilized to calculate AOD measurements at multiple wavelengths, as described by O'Neill et al. (2003) and verified by Kaku et al. (2014). The Dubovik et al. (2000) column-integrated fine and coarse mode aerosol size distribution at ambient RHs also were used during the analyses for those cases that passed level 2 quality assurance: Particle size distributions are considered valid for AOD requirements that at a wavelength of 440 nm, AOD $>$ 0.1, but inversions of index of refraction and absorption require 440 nm AOD $>$ 0.4. Due to the screening processes applied to the level 2 data and occasional equipment malfunction, all sites experienced outages. The CTR data end after 17

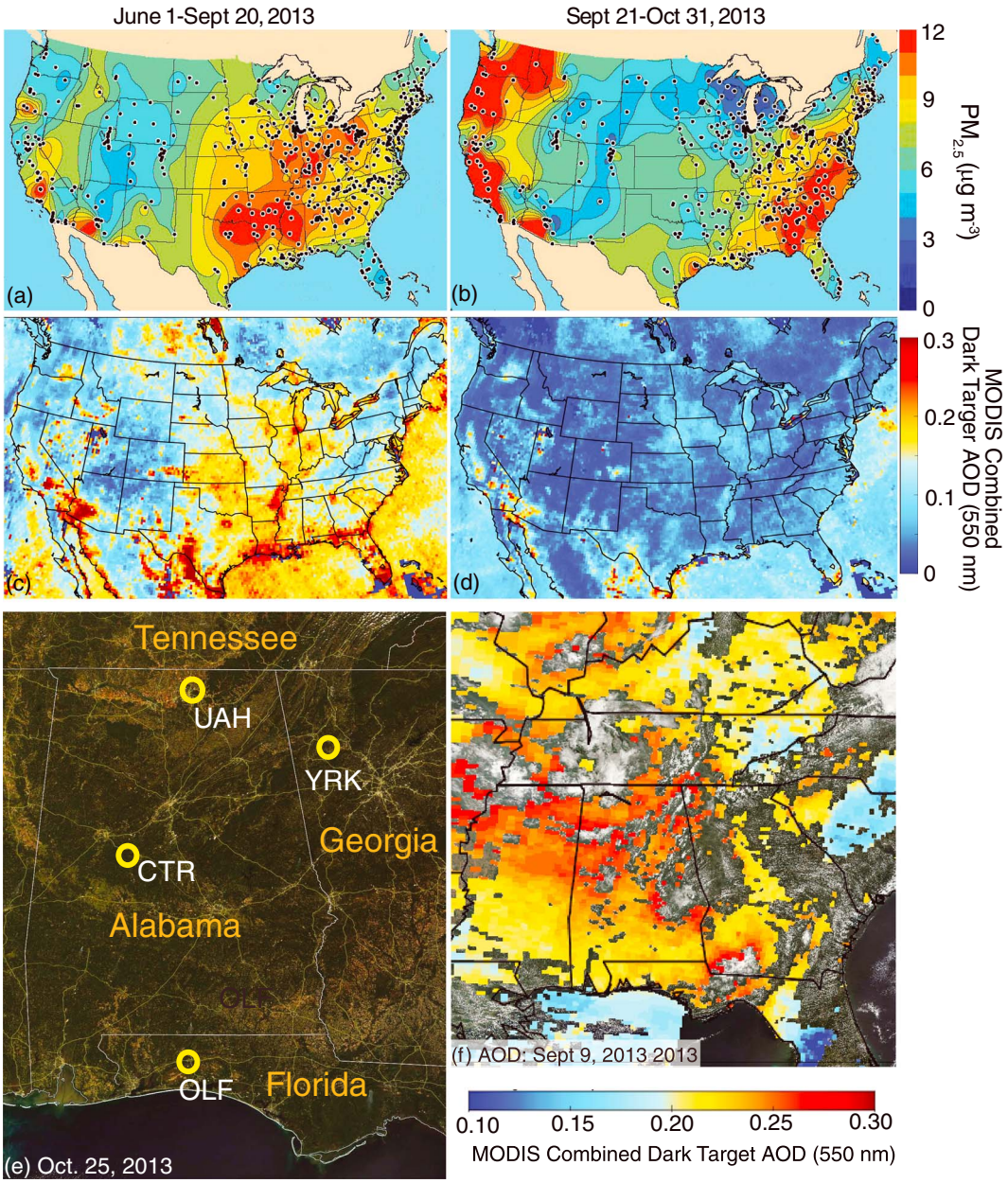

Figure 1. The observed EPA-FRM kriged $PM_{2.5}$ mass concentrations data for (a) the summer regime of the SEAC^{4}RS data set (1 June to 20 September 2013) and (b) the fall-regime (21 September to 31 October 2013), with Huntsville marked. The box refers to the study area of this paper. The corresponding Terra MODIS 550 nm AOD observed during (c) the summer and (d) fall regime. A (e) NASA Blue Marble map of the SEARCH and CSN sites (CTR: Centreville; OLF: Outlying Landing Field; UAH: Univ. Alabama Huntsville; YRK: Yorkville) utilized in this analysis and (f) an overlaid on Terra MODIS level 2 combined dark target AOD product of the mission's most significant air quality event 9 September 2013.

September; OLF is missing data for a week starting 16 June and has only one day of data between 15 July and 26 August. YRK has three outages: eight days starting 5 June, 11 days starting 16 June, and almost the entire month of August.

2.2. $PM_{2.5}$ Mass and Chemistry

Data from the SEARCH network were utilized (Edgerton et al., 2005; Hansen et al., 2003) to determine the surface $PM_{2.5}$ aerosol mass, chemistry, and extinction at the CTR, OLF, and YRK sites. The SEARCH sites were recently decommissioned, but the data can currently be accessed at http://views.cira.colostate.edu/fed/

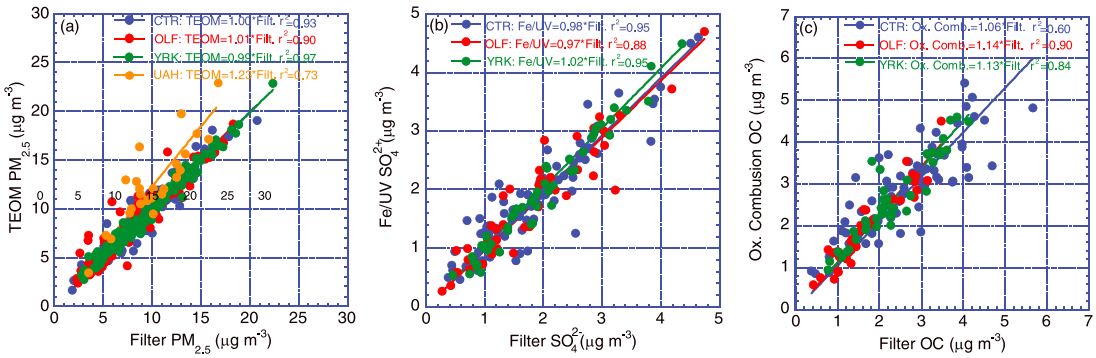

Figure 2. Comparison of the daily-averaged 5-min resolution of $PM_{2.5}$ aerosol mass and chemistry to the 24-hr resolution filter analysis of mass and chemistry for (a) $PM_{2.5}$, (b) sulfate ion, and (c) organic carbon (OC). Data for different sites are plotted in different colors with associated bias and calculated coefficients of determination shown.

DataWizard/Default.aspx. While only three sites are utilized in this paper, the recently decommissioned SEARCH network consisted of eight sites in Georgia, Alabama, Mississippi, and Florida, and each site contained a similar suite of instruments to measure surface-level aerosol mass. The measurements relevant to this paper include continuous $PM_{2.5}$ mass using tapered element oscillating microbalance (TEOM) and chemistry including sulfate (SO_4^{2-}), total carbon (TC) and organic carbon (OC), 24-hr aerosol filter collection, and analysis comprising of gravimetry, ion chromatography, and thermal/optical reflectance and transmittance (TOR/TOT) analysis. $PM_{2.5}$ filters at the SEARCH sites were equilibrated at 21 °C and 35% RH, suggesting low potential for contribution from water to the $PM_{2.5}$ mass. Light scattering and absorption ($\sigma_{sp,dry}$, $\sigma_{ap,dry}$) were measured at a dry RH ~ 20% using a nephelometer and aethalometer, respectively. More details on the collection methods and can be found in Table 1 and in Hansen et al. (2003). The SEARCH-CTR site is notably a center of extensive study for the SENEX campaign and aptly named as the center of our study activity.

To demonstrate confidence in the finer scale temporal resolution, we compared the 24-hr average of the 5-min resolution $PM_{2.5}$ chemistry with its corresponding daily filter analysis from June through October 2013. The 24-hr averages were made on the hour, with no data filtering as the quality control was performed on the data a priori before the data are published. Figure 2 shows a strong correlation between the higher frequency measurements with the filter analysis, with low root-mean-square errors (RMSE) and biases for the total $PM_{2.5}$ mass, sulfate concentration, and OC concentration. Thus, we have confidence using both the high resolution and the 24-hr aerosol chemistry measurements at the three SEARCH sites. There are low offsets for all variables, ranging from 0.1 to 0.8 μg/m^3 for comparisons of the filter mass to the TEOM mass, 0.1 to 0.3 μg/m^3 for sulfate, and 0.1 to 0.8 μg/m^3 for comparisons of OC. The UAH site mass comparison experienced the largest offset of 1.2 μg/m^3. The UAH CSN filter $PM_{2.5}$ mass may be biased high as they are weighed at an RH ~ 40%, as per EPA protocol (Malm et al., 2011), 5% higher than the SEARCH sites data collection protocol, thus retaining more water than the SEARCH filters.

Five kilometers from the UAH site, the CSN site, located at the Huntsville Old Airport, collected data on $PM_{2.5}$ aerosols, including $PM_{2.5}$ gravimetric mass, ions, elements, and carbon (organic and elemental) species (available at http://www.airnowtech.org/). While the site provides continuous TEOM $PM_{2.5}$ mass measurement data (Table 1) for $PM_{2.5}$ aerosol mass, it also measures filter mass every three days, and $PM_{2.5}$ speciation every six days, providing information on sulfate, nitrate, sodium, potassium, ammonium, and OC and black carbon (BC) mass as specified by the FRM methodology (https://www3.epa.gov/ttnamti1/speciepg.html, last accessed 15 March 18). Unlike the SEARCH filter data, the OC mass was not blank corrected, and thus, 0.3 μg/m^3 was subtracted from the OC mass to account for background concentrations on the filters (Hand et al., 2012). Both the ammonium at the CSN site and nitrate at all sites are subject to significant negative artifacts due to volatilization, although nylon filter measurements at all sites minimized the loss (Hering & Cass, 1999; Yu et al., 2006).

2.3. Satellite

Satellite observations of operational Collection 6 dark target 550 nm AOD were collected from the MODIS aboard Terra and Aqua, with overpasses over UAH at ~15:30/10:30 and 18:30/13:30 UTC/LDT (local daily

time) daily (Levy et al., 2013). The dense vegetation covering much of SEUS provides a higher level of confidence for the MODIS retrieval (Roy et al., 2007). AOD cloud fraction measurements were analyzed. Also used are v22 AOD retrievals from the MISR instrument on Terra (Kahn et al., 2005). For MISR AOD data, only successful retrievals as indicated by the QA flag are used in the analysis and no cloud screen is applied. Satellite retrievals with cloud fraction above 25% were screened out to prevent high bias in the results. Daily yields of observations for satellite AOD retrievals at individual sites were relatively low, at 20–40% for Terra and Aqua MODIS observations (due to retrieval failure for high cloud cover), and 4–9% for MISR (with the inclusion of one day in seven sampling). Between both MODIS sensors, there is an ~50% chance of an observation at each site on a given day over the study period. All available 10 km resolution MODIS DT (with QA flag of above or equal to 1) as well as all available MISR (successful retrievals as indicated by the QA flag) AOD data were used for the study period.

2.4. UW-HSRL

Core to the SEAC^{4}RS ground component were facilities in association with the University of Alabama, Huntsville. The UW-HSRL was operational 18 June to 4 November 2013 at the UAH NSSTC Regional Atmospheric Profiling Center for Discovery (RAPCD: 34.72°N; 86.64°W, 100 m above mean sea level). Aerosol properties, including backscatter and aerosol depolarization, were collected using a frequency-doubled diode-pumped neodymium: yttrium/aluminum/garnet (Nd:YAG) laser operating at 532 nm wavelength at a collection rate of 4 kHz. Aerosol backscatter coefficients, collected at altitudes of roughly 100 m to 15 km, are corrected for the molecular attenuation, and, with knowledge of the derived lidar ratio (S_a), can be converted to aerosol extinction coefficients. This instrument can provide highly precise estimates of aerosol backscatter, at $<$10% of the Rayleigh backscatter signal. Due to signal-to-noise ratios and uncertainties in the geometric factors, HSRL extinction measurements have a lower limit of 1×10^{-4}/m. As discussed in Reid et al. (2017) a mean S_a of 55 sr is able to reproduce the AERONET column AOD within 20%.

2.5. Other Ancillary Data

Located at all three SEARCH sites as well as at the UW-HSRL at the NSSTC/RAPCD site were a host of instruments to monitor the atmosphere including weather station tracking temperature, pressure, and RH.

3. Results I: Chemical and Optical Properties for Core Sites

To provide a baseline of aerosol variability throughout the SEUS air quality region, here we present the analysis the AOD and $PM_{2.5}$ observations made at the three SEARCH sites and at the UAH site during the SEAC^{4}RS ground campaign. An overview of the regional meteorology and aerosol vertical distribution of the SEUS is incorporated into Reid et al. (2017) and not reproduced here. However, some key aspects will be provided as required in this section. In summary, the summer 2013 deployments largely occurred in a summertime convective regime from June through mid-September. Fair weather summertime days were frequent, with ~50% cumulus coverage. Weak fronts regularly passed through the region, bringing with them deep convection. By 20 September, the regime changed to more autumn frontal activity with lower overall AOD and temperatures. Summertime fair weather days exhibited classic PBL structure: an ~1.2 km above ground level deep mixed layer accounting for ~50% of AOD and a cumulus filled entrainment zone providing another 25%. This entrainment zone was often capped by large-scale subsidence at ~2.5 km above ground level, but sometimes reached as high as 0 °C/~4.5 km in more convectively active regimes. The remaining AOD was attributed to the lower free troposphere from either convective detrainment or frequent intrusions of western U.S. biomass burning smoke. Occasional strong injections of smoke to the upper troposphere also strongly perturbed AOD, particularly in late June.

Baseline data for the 2013 summer aerosol season are provided in Table 2, and time series of $PM_{2.5}$ component mass concentrations (total $PM_{2.5}$, sulfate, OC, soils, and BC) for the sites are provided in Figure 3, along with their intercorrelation between each site and CTR. The soil calculation follow the IMPROVE algorithm of 2.2*Al + 2.49*Si + 2.42*Fe + 1.94*Ti + 1.6*Ca and sea salt is calculated using 1.8*Cl^- (Malm & Hand, 2007), although this method tends to underestimate sea salt concentrations due to chloride depletion. Subsequent time series and intercorrelation of mass fraction, optical properties, and AERONET derived properties are likewise included from Figures 4–9. For simplicity here, we conduct this baseline analysis largely from the context of daily mean properties, with the understanding that AERONET is limited to daytime

Table 2
Bulk Mean Site Statistics for Air Quality Sites Examined for the June–October 2013 Study Period

	CTR	OLF	YRK	UAH*
$PM_{2.5}$				
Number of measurements	133	134	145	148
$PM_{2.5}$ (μg/m^3)	8.6 ± 3.5	8.1 ± 3.8	9.4 ± 3.9	12.2 ± 5.5
$PM_{2.5}$ 10th/90th % (μg/m^3)	4.1/12.8	3.6/13.8	4.6/14.6	7.3/18.2
$PM_{2.5}$ min/max (μg/m^3)	1.9/20.7	2.3/18.3	2.8/22.4	3.4/28.7
$PM_{2.5}$:PM_{10}	0.57 ± 0.09	0.55 ± 0.13	0.64 ± 0.15	0.59 ± 0.09
$PM_{2.5}$ SO_4^{2-} (%)	23 ± 8	23 ± 8	22 ± 5	21 ± 6
$PM_{2.5}$ $NH_4^{+:}$ (%)	7 ± 3	7 ± 3	7 ± 2	5 ± 2
$PM_{2.5}$ OC (%)	31 ± 10	20 ± 7	25 ± 6	22 ± 5
$PM_{2.5}$ POM (%)	56 ± 18	36 ± 11	44 ± 10	39 ± 8
$PM_{2.5}$ black carbon(%)	4 ± 2	4 ± 2	4 ± 1	2 ± 1
$PM_{2.5}$ NO_3^- (%)	1 ± 1	2 ± 1	3 ± 2	4 ± 4
$PM_{2.5}$ sea salt (%)	0 ± 0	1 ± 3	0 ± 0	0 ± 0
$PM_{2.5}$ dust/soil (%)	7 ± 9	24 ± 25	7 ± 10	5 ± 4
$PM_{2.5}$ residual (%)	2 ± 22	3 ± 21	15 ± 11	25 ± 8
SO_4:OC	0.8 ± 0.5	1.3 ± 0.9	0.94 ± 0.35	1.1 ± 0.5
Optical and environmental properties				
σ_{sp} (Mm^{-1})	32 ± 17	19 ± 11	34 ± 19	N/A
α_{sp}, (m^2/g)	3.7 ± 0.8	2.3 ± 0.5	3.6 ± 0.6	N/A
σ_{ap} (Mm^{-1})	5.1 ± 2.6	5.1 ± 2.2	5.6 ± 2.5	N/A
α_{ap}, (m^2/g)	0.6 ± 0.2	0.7 ± 0.2	0.6 ± 0.2	N/A
α_{ext}, (m^2/g)	4.2 ± 0.8	2.9 ± 0.6	4.2 ± 0.8	N/A
ω_o	0.86 ± 0.05	0.77 ± 0.06	0.85 ± 0.05	N/A
$\alpha_{sp,spec}$ (m^2/g)/r^2	4.5/0.86	2.6/0.81	4.7/0.88	N/A
$\alpha_{ap,spec}$ (m^2/g)/r^2	0.55/0.51	0.45/0.55	0.62/0.51	N/A
Linear reconstructed ω_o	0.90	0.85	0.90	N/A
Relative humidity (%)	79 ± 8	83 ± 8	82 ± 8	69 ± 8

Note. The $PM_{2.5}$ mass and chemistry are from 24-hr filter measurements, and the optical statistics are based on daily averages, except for UAH data, which is one day in six. Dry scattering coefficients (σ_{sp}) and mass scattering efficiencies (α_{sp}) were measured at 530 nm. Dry absorption coefficients (σ_{ap}) and mass absorption efficiencies and (α_{ap}) were measured at 580 nm. Regressions were used to measure $\alpha_{sp,spec}$ and $\alpha_{ap,spec}$, and point-wise analysis were used to derive α_{sp} and α_{sp}. Unless otherwise stated, the statistics presented are mean ± standard deviation. The particulate organic matter (POM) to organic carbon (OC) assumes a ratio of 1.8. The soil/dust calculation assumes the same oxides as the IMPROVE algorithm of 2.2*Al + 2.49*Si + 2.42*Fe + 1.94*Ti + 1.6*Ca and sea salt is calculated using 1.8*Cl^- (Malm & Hand, 2007).

only, and satellite retrievals are at best once per day. These higher frequency sampling issues are discussed in section 3.3.

3.1. $PM_{2.5}$ Mass and Chemistry

The time series of daily $PM_{2.5}$ and its key components are provided in Figure 3. Mean values for $PM_{2.5}$ for CTR, OLF, YRK, and UAH sites were within one standard deviation of one another for the study period at 8.6 ± 3.5, 8.1 ± 3.8, 9.4 ± 3.9, and 12.2 ± 5.5 μg/m^3, respectively. Daily-mean values for all sites ranged from under 2 μg/m^3 during wet convective periods or post frontal passage to the greater than 20 μg/m^3 for the most significant haze periods. The highest 24-hr maxima were observed for events on 30 August and 9 September, with sites reporting 18–22 μg/m^3 across the region. In context, the U.S. National Ambient Air Quality Standards (NAAQS) 24-hr $PM_{2.5}$ standard of 35 μg/m^3 was not exceeded during this study period. On average, $PM_{2.5}$ accounted for ~55–64% of PM_{10} total mass at all sites.

Temporally, while $PM_{2.5}$ variability at the daily level is clearly visible in Figure 3a, especially in early June, overall $PM_{2.5}$ tends to have significant structure over many days to a week timescale. Simple *e*-folding autocorrelation times of $PM_{2.5}$ were on the order of three days for all four sites. With the exception of the CTR-OLF relationship, sites also showed reasonably good agreement to one another at the daily level, with r^2 values to CTR of 0.34, 0.63, and 0.61 to OLF, YRK, and UAH, respectively. The highest daily $PM_{2.5}$ averages as well as the greatest seasonal concentrations were experienced at the suburban UAH site, with the most significant events occurring in late August through early September. This is consistent with previous studies,

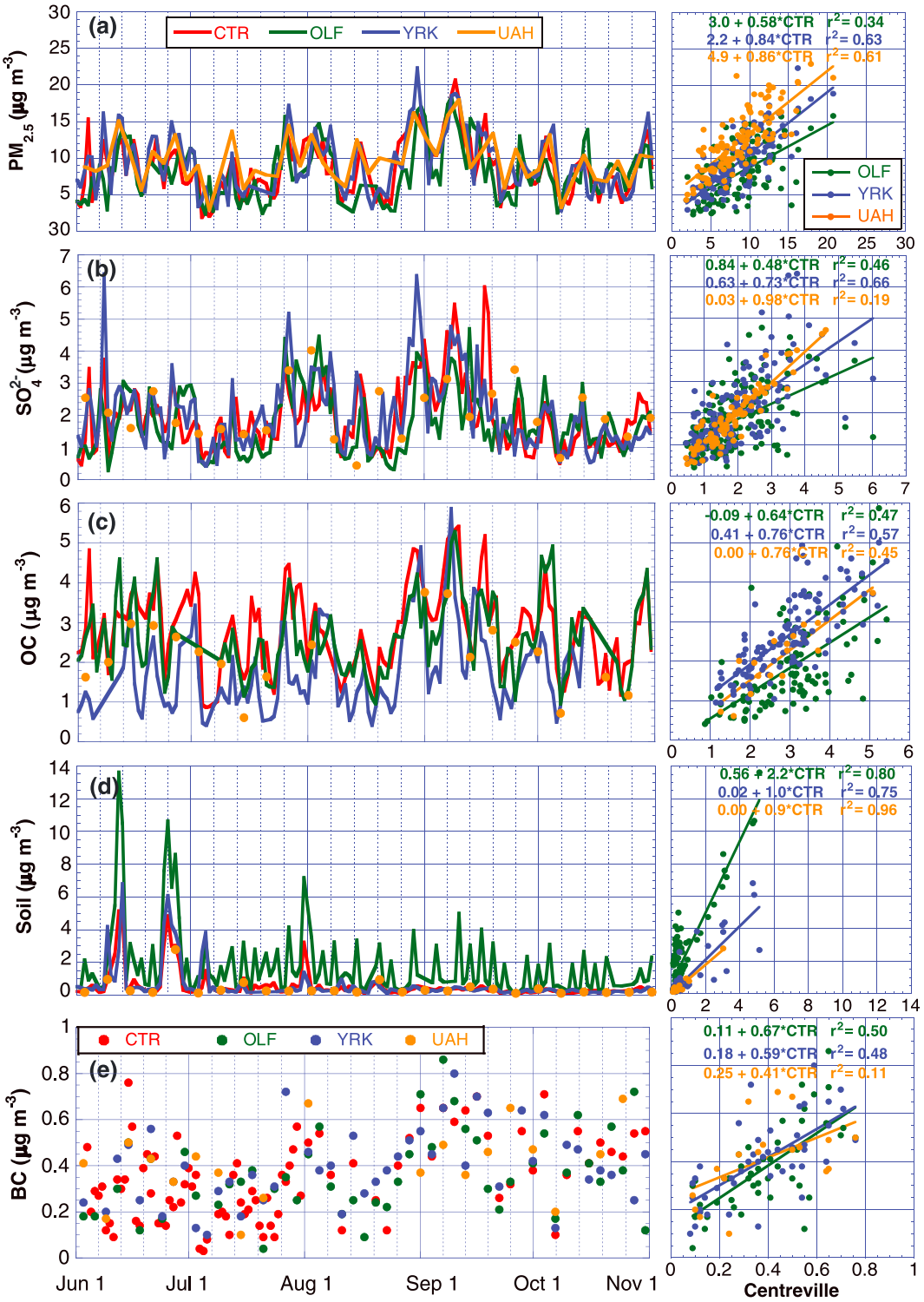

Figure 3. Time series of daily ground based extensive parameters used in this study. Also shown are the scatter plots with linear regression equations of these parameters to Centreville, which share y-axes labels with the time series plots. Included are 24-hr filter-measured surface (a) $PM_{2.5}$, (b) sulfate (SO42-), (c) organic carbon (OC), (d) soils, and (e) black carbon (BC) concentrations. Sites include the following: CTR: Centreville AL, OLF: Outlying Field FL, YRK: Yorkville GA, UAH: University of Alabama Huntsville, AL. At UAH chemistry is one day in six.

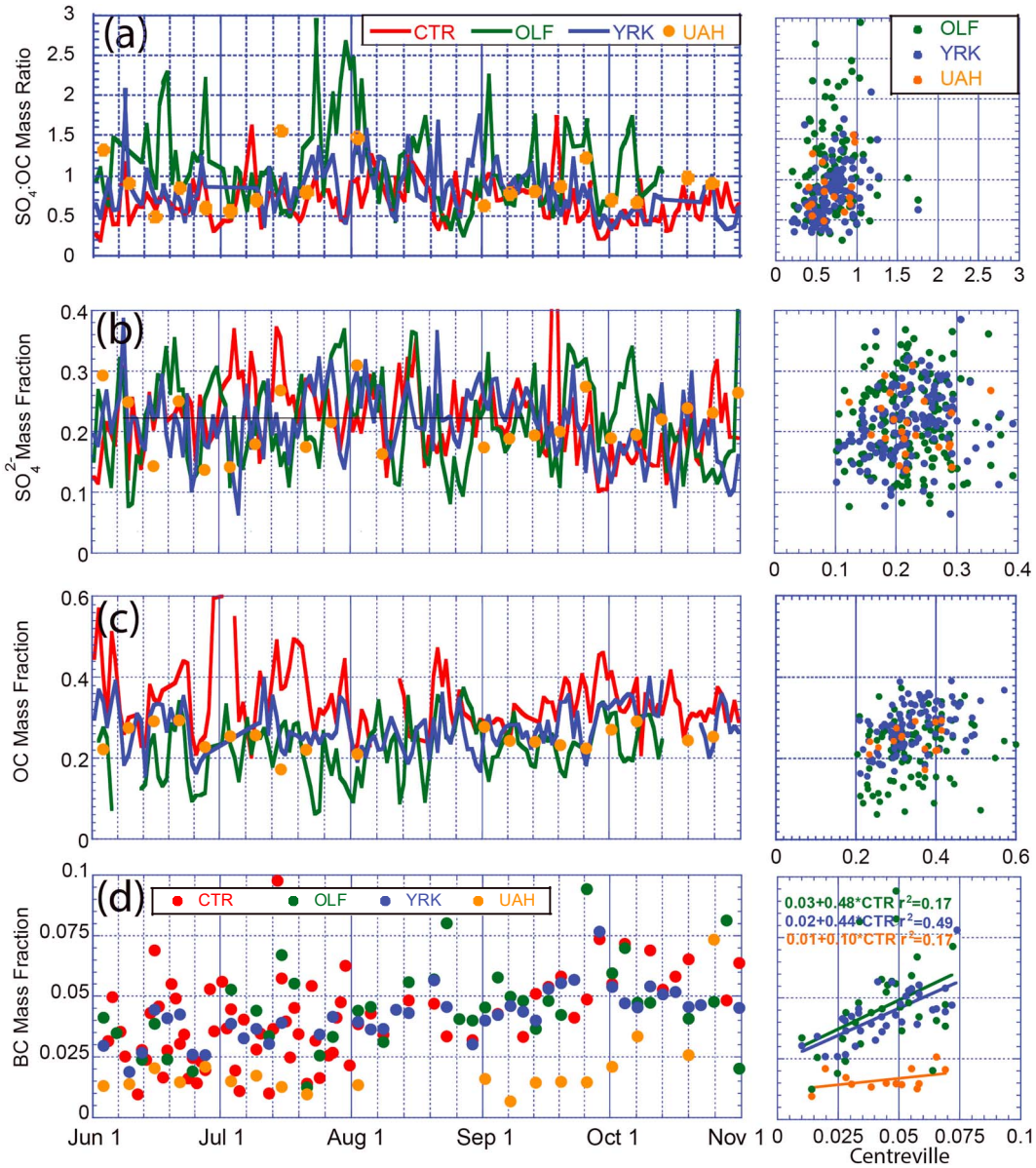

Figure 4. As in Figure 3 but for mass fractions observed at the four sites. Included are 24-hr filter-measured surface (a) sulfate to organic carbon ratios SO4:OC, (b) sulfate (SO_4^{2-}), (c) organic carbon (OC), and (d) black carbon (BC) mass ratio with corresponding scatter plots against Centreville. Sites: CTR: Centreville, AL, OLF: Outlying Field, FL, YRK: Yorkville, GA, UAH: University of Alabama Huntsville, AL. UAH chemistry is one day in six. The scatter plots in subplots (a) through (c) show no significant correlations. The times series and the scatter plots share *y* axes.

corresponding to summer-time peaks in biogenic emissions, which mix with anthropogenic emissions in a humid environment resulting in significant secondary particle production (Ford & Heald, 2013; Weber et al., 2007). As discussed in Reid et al. (2017), the SEUS shifted from a convective to more of a fall like and cooler frontal environment after 20 September, reducing biogenic emissions and haze. The four sites studied here represent the same SEUS region, whose summer month aerosol composition is expected to be similarly dominated by secondary organic aerosols (SOAs) and anthropogenic sulfate aerosols (Ford & Heald, 2013), with additional contributions from other trace species. Time series and tabular data are also presented in Figure 3 and Table 2, respectively. The SEARCH/CSN filter results confirm organic carbon and sulfate ion dominated aerosol mass during the SEAC^{4}RS campaign. While the sulfate mass fraction was fairly consistent across the sites (21–23%), CTR had a markedly higher OC mass fraction (31%) versus 20–25% for the other sites. This may be a result of its location as the most rural of areas investigated here.

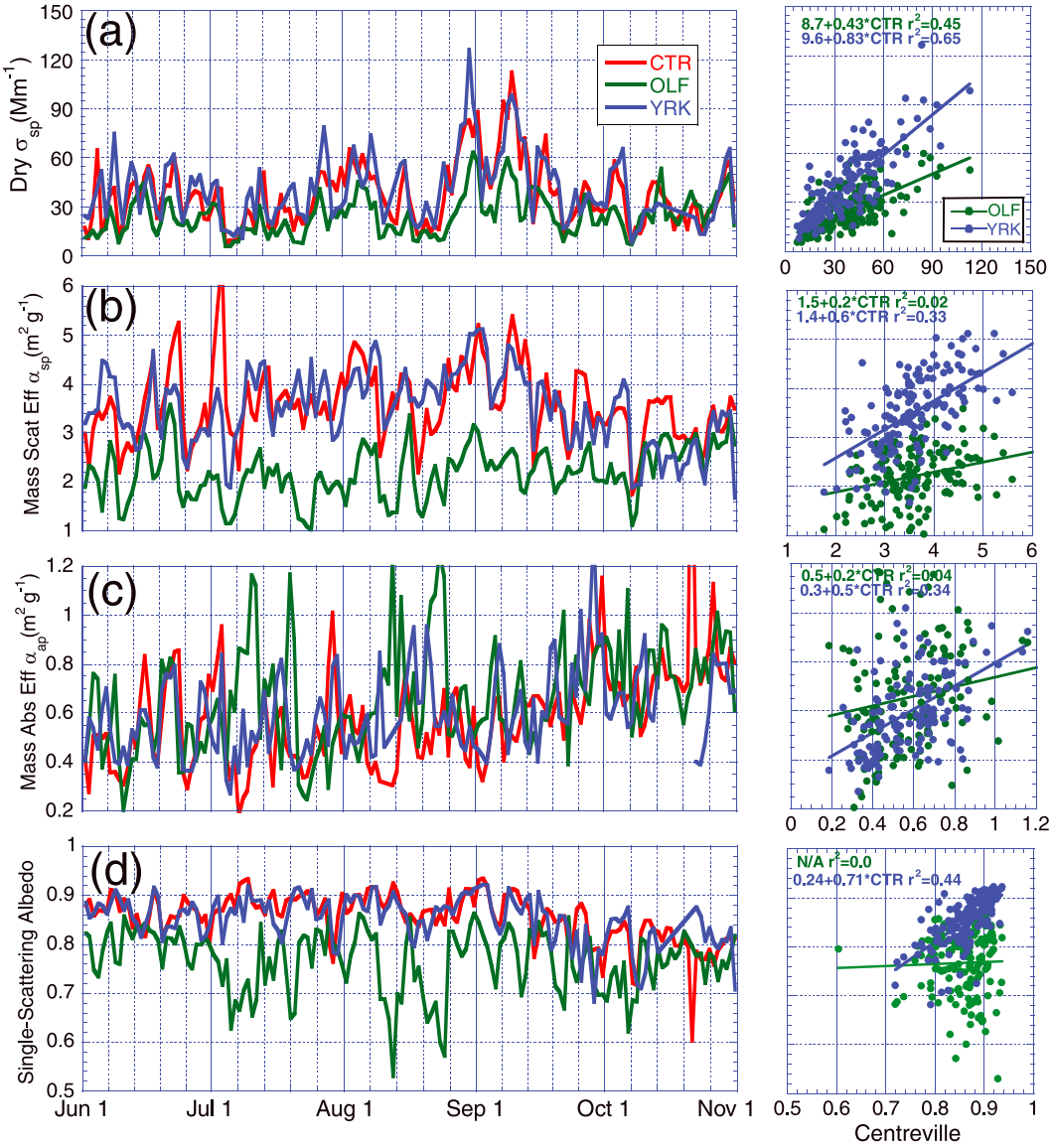

Figure 5. As in Figure 3 but for optical properties observed at the three SEARCH sites. Included are daily average surface (a) dry scattering coefficients (σ_{sp}; λ = 530 nm), (b) mass scattering efficiency (α_{sp}), (c) mass absorption efficiency (α_{ap}; λ = 565 nm), and (d) single-scattering albedo (ω_o) with corresponding scatter plots against Centreville. The scatter plots share *y* axis labels with the time series plots on the left.

The stoichiometric ratio of NH_4^+ and SO_4^{2-} was 1.7 at all SEARCH sites, suggesting a combination of ammonium sulfate and ammonium bisulfate. The UAH site yielded a stoichiometric ratio of 1.4, but this must be interpreted with caution due to the known ammonium volatilization problem associated with the CSN sites (Yu et al., 2006). If one assumes that all ammonium is associated with the sulfate, and the ratio of particulate organic matter (POM) to OC is 1.8, as is used in the IMPROVE network (Malm & Hand, 2007), then POM and ammonium sulfates account for 86%, 66%, 73%, and 65% of total $PM_{2.5}$ at CTR, OLF, YRK, and UAH, respectively. Temporally, total $PM_{2.5}$ mass as well as the SO_4^{2-} and OC mass components started to drop in the early fall season (after 20 September), as is expected for the region (Hand et al., 2012).

The next most dominant species was soils. Common oxides of Si, Al, Fe, Ti, and Ca (Malm et al., 1994), presumably soils/dust, account for 5–24% of the $PM_{2.5}$ mass. Derived soils were in general very low in the SEUS (~ 0.5 μg/m^3) with the exception of three multiday events spanning the region, centered on 11 and 26 June which peaked at ~20–40% of the $PM_{2.5}$ mass. Highest soil concentrations and mass fractions were

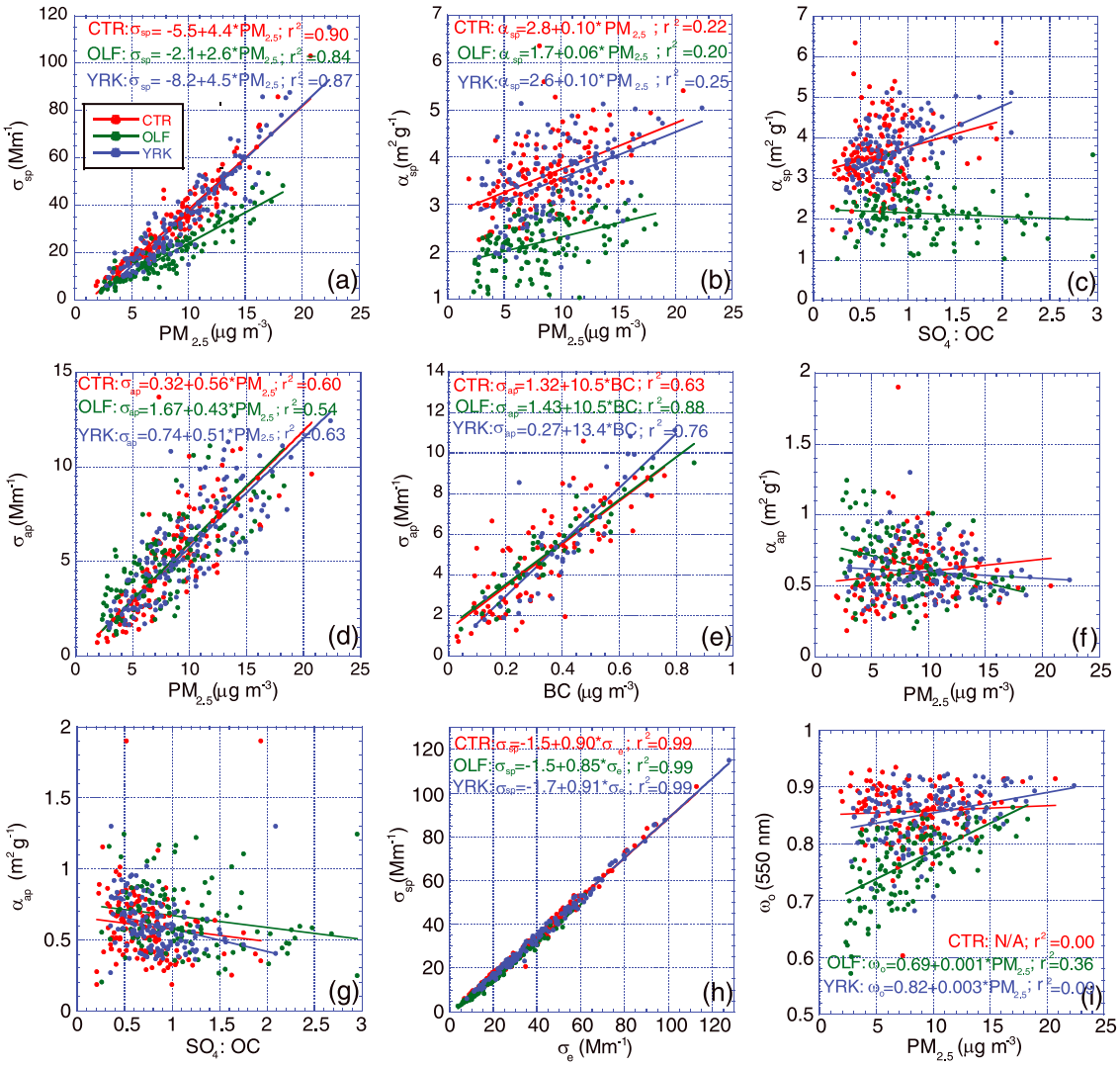

Figure 6. Scatter plots of surface-level aerosol optical properties and aerosol mass and chemistry, including single-scattering albedo (ω_o), dry aerosol scattering coefficient (σ_{sp}), dry absorption coefficient (σ_{ap}), extinction coefficient (σ_e) mass scattering efficiency (α_{sp}), and mass absorption efficiency (α_{ap}) and mass extinction efficiency (α_{ext}). Scattering coefficient measurements were made at λ = 530 nm and absorption efficiency measurements λ = 565 nm. Linear relationships are described on the subplots when significant.

at the southern coastal OLF site. The International Cooperative for Aerosol Prediction (ICAP) multimodel ensemble (Sessions et al., 2015), NAAPS reanalysis (Xian et al., 2016), and aerosol chemistry filter analysis (Hand et al., 2017) indicate that these events are due to intrusions of African dust.

BC accounts for an additional 4% of $PM_{2.5}$ mass at the SEARCH sites, which was also relatively well correlated to CTR (Figure 3e) as well as with OC (r^2 = 0.39, 0.78, and 0.74 at the CTR, OLF, and YRK sites, respectively). UAH was an outlier in this regard, with markedly lower BC concentrations and mass fractions, even if one compares a pairwise matched data set with SEARCH. Other trace mass species include nitrate at 1–4% of the mass budget. Sea salt is 0–1% even at the more coastal OLF site, although this is likely an underestimation due to the chloride that is lost during atmospheric processing (Kerminen et al., 1998). Taking all of these into account, we are left with roughly 2–25% of unexplained residual, with the largest unexplained mass being associated with the CSN data at Huntsville. While some of the residual may be due to assumptions made in calculating POM and soils, some is due to bias in $PM_{2.5}$ gravimentric measurements including particle-bound water on the filter or reactions with atmospheric gases (Malm et al., 2011). Overall, these findings are consistent with previous campaigns that show summertime aerosol mass of the SEUS dominated by FM biogenic SOAs and anthropogenically produced sulfate aerosols (e.g., Hand et al., 2012; Hansen et al., 2003; Weber et al., 2007).

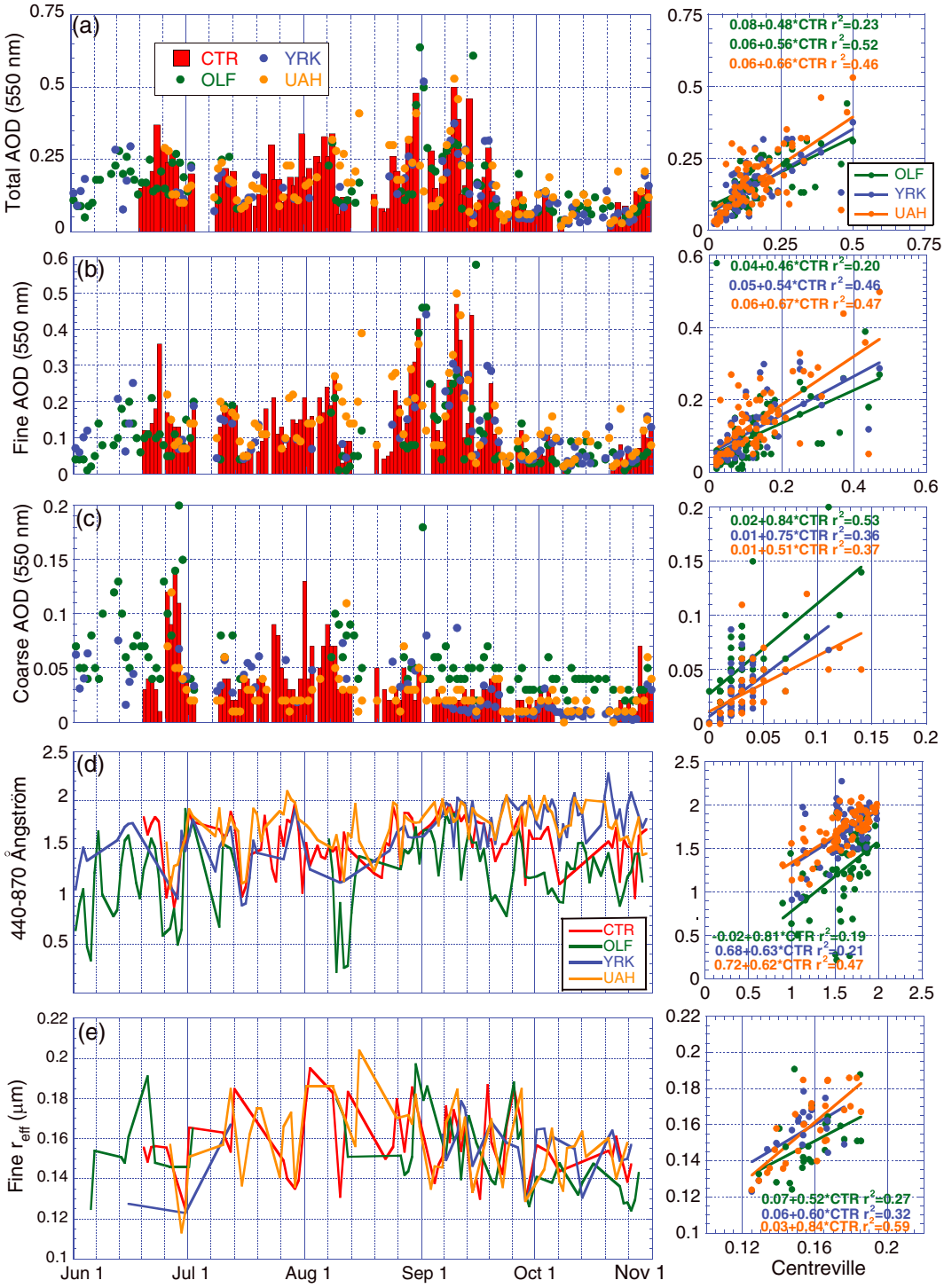

Figure 7. AERONET-measured AODs and AERONET products observed during the SEAC^{4}RS campaign. Included are (a) total 550 nm AOD, (b) fine mode AOD, (c) coarse mode AOD, (d) 440–870 nm Ångström coefficient, and (e) the inversion-derived fine mode effective radius.

Clearly the dominant drivers of $PM_{2.5}$ variability were OC and SO_4^{2-}. These species were moderately correlated with one another (r^2 between 0.36 and 0.48 at all sites) although the ratio of sulfate to OC was not in general related to $PM_{2.5}$ concentration. The ratio of SO_4^{2-} to OC was highly variable temporally and spatially with no intersite correlation on a day-to-day basis (Figure 4a), yet the SO_4:OC ratio systematically dropped,

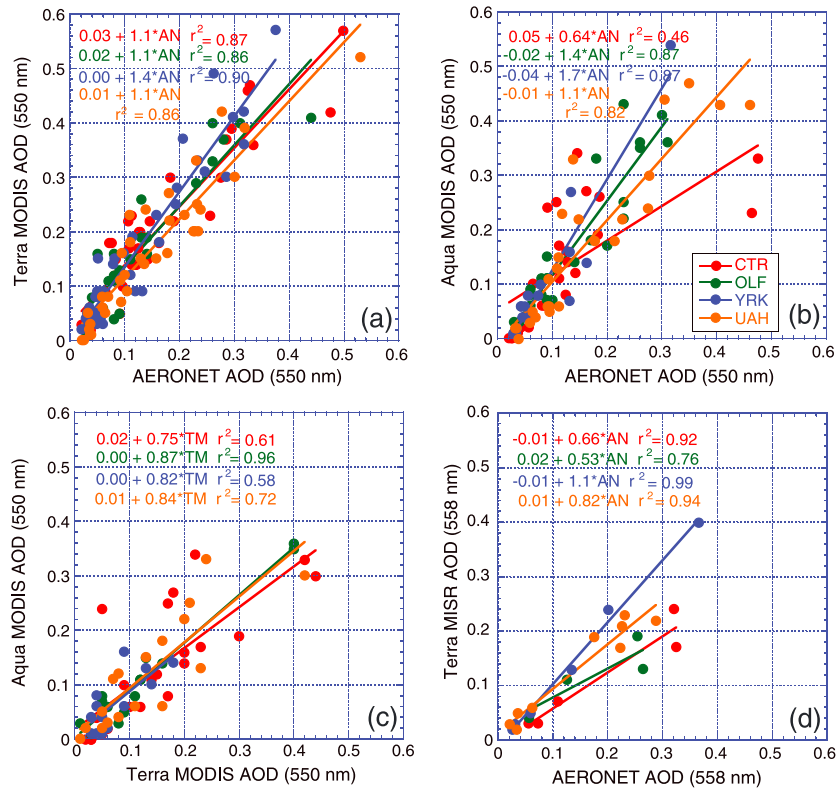

Figure 8. Scatter plots with linear regressions between measured AODs at the four sites during the SEAC^{4}RS campaign including the derived 550 nm AERONET AOD, the Aqua and Terra MODIS 550 nm AOD, and the Terra MISR 558 nm AOD. Regression equations against the AERONENT AOD (AN) and Terra MODIS (TM) are shown on the subplots.

once more fall-like weather began in late September, primarily due to an increase in the OC mass fraction, and a slight decrease in the SO_4^{2-} mass fraction (Figures 4b and 4c). At the same time, BC concentrations and mass fractions also increased after late September (Figure 4d).

While sulfate and OC are expected to have to some extent different primary sources, namely, anthropogenic emissions and biogenic emissions, secondary aerosol formation pathways are linked, that is aquatic chemistry and photochemical reactions. While the formation of organosulfate SOA can explain some of the correlation, Zheng et al. (2002), suggested that the majority of the OC at the SEARCH sites in the summer months is due to diesel emissions and not biogenic emissions, which would also lead to a connection between SO_4^{2-} and SOA within the $PM_{2.5}$ mass, although the research of Zheng et al. (2002) was performed prior to the switch to ultralow sulfur diesel fuel post 2006, which may render their proposed link less viable (https://www.epa.gov/diesel-fuel-standards/diesel-fuel-standards-and-rulemakings; last accessed 15 March 2018). Similarly, Malm et al. (2017) found a significant decrease in SOA concentrations corresponding to declines in SO_4^{2-} since 2001, suggesting a dependence of the SOA formation mechanisms on SO_4^{2-} $PM_{2.5}$ concentrations. Thus, it is not completely correct to assume sulfate and OC as orthogonal components of the $PM_{2.5}$ mass. However, reconstruction of $PM_{2.5}$ mass can be achieved using only the three dominant components (OC, sulfate, and soils). By multiple linear regressions at all sites, we find

$$\text{All sites}: PM_{2.5} = 2.3\ SO_4^{2-} + 1.6\ OC + 0.30\ Soil + 0.34; r^2 = 0.87, N = 206 \quad (3)$$

$$\text{CTR}: PM_{2.5} = 2.4\ SO_4^{2-} + 1.4\ OC + 0.18\ Soil + 0.01; r^2 = 0.87, N = 86 \quad (4)$$

$$\text{OLF}: PM_{2.5} = 1.8\ SO_4^{2-} + 2.6\ OC + 0.52\ Soil + 0.28\ r^2 = 0.96, N = 47 \quad (5)$$

$$\text{YRK}: PM_{2.5} = 2.2\ SO_4^{2-} + 2.1\ OC + 0.64\ Soil - 0.30; r^2 = 0.97, N = 47 \quad (6)$$

$$\text{UAH}: PM_{2.5} = 1.4\ SO_4^{2-} + 2.4\ OC + 1.2\ Soil + 0.85; r^2 = 0.76, N = 26 \quad (7)$$

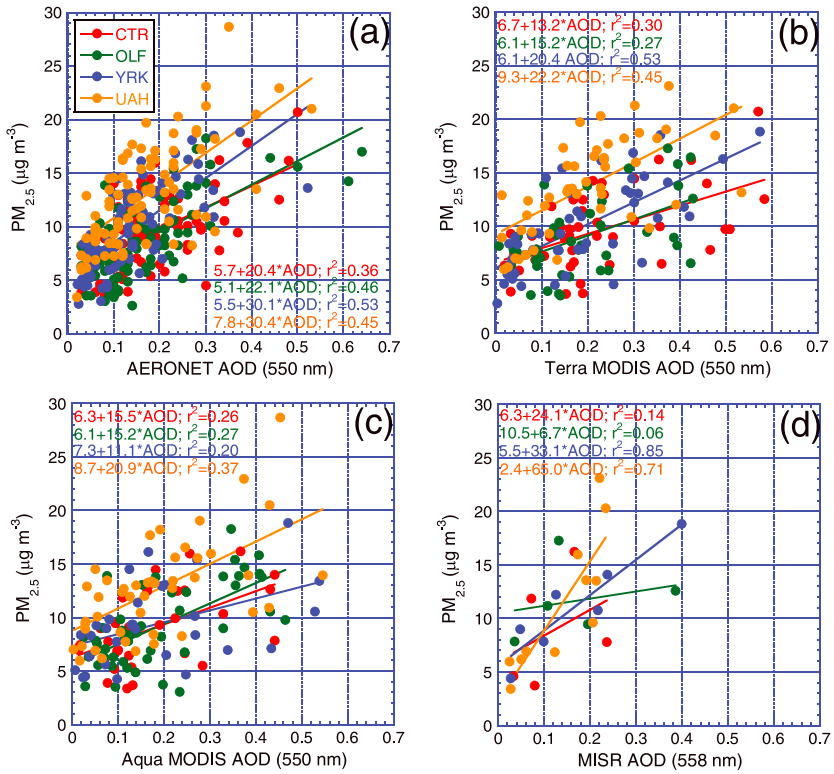

Figure 9. A visualization of the linear relationship between the 24 hr-averaged surface-level $PM_{2.5}$ mass and the measured AODs derived from (a) AERONET, (b) the Terra MODIS, (c) the Aqua MODIS, and (d) the Terra MISR.

Overall the multiple regression equations using only organic carbon, sulfate, and soil account for covariability with other species and capture most of the total $PM_{2.5}$ mass reconstruction and mass variability at the four sites, with high r^2 values and low constants within each of the four equations. Interpretation of individual regression formulations should proceed with caution, however. Malm and Hand (2007) assessed that regression results can be impacted by measurement uncertainties, which would be higher for organics than sulfates, producing an underprediction for the coefficient associated with the OC term, and an overprediction for the sulfate term. Furthermore, even at low humidities, ammonium sulfate will be associated with some tightly bound water, contributing to a higher coefficient. As discussed above, the OC and SO_4^{2-} components are not completely orthogonal.

Even with these caveats, it is of note that the site-based regression analyses produced markedly different results at each site. The assumed mass multiplier for fully neutralized ammonium sulfate is 1.375 SO_4^{2-}. The UAH site SO_4^{2-} multiplier approaches this value, but the SEARCH sites considerably exceed it, perhaps due to bound water, as discussed above.

The OC term as an indicator species appears to play a greater role at the OLF and UAH sites, and despite its higher mass fraction, a lesser role at the forested CTR site. Again, this suggests that the majority of the organic mass in the region could be due to anthropogenic sources rather than biogenic emissions, and supports recent findings suggesting the formation of OC and SO_4^{2-} in $PM_{2.5}$ are linked (Malm et al., 2017; Schichtel et al., 2017). The OC multiplier can also be interpreted as reflecting the amount of oxidation within the POM. Regionally, with an "all sites" coefficient of 1.6, the organics appear to be slightly less oxidized than suggested by the IMPROVE multiplier of 1.8, but within the accepted range of 1.2 and 2.0 (Malm et al., 2011). However, this varies significantly from site to site, with all sites except CTR showing highly oxidized POM.

While SO_4^{2-} is less dominant than the OC mass fraction within the SEARCH sites, it is on par with or dominant to the OC term in the multiple regression equations. However, when looked at in terms of a single regression, sulfate and OC play equal importance, perhaps reflecting their covariance in the atmosphere, as discussed above. Indeed, simple regressions of to SO_4^{2-} to $PM_{2.5}$ were found to have r^2 = 0.72, 0.77, and 0.76 for

CTR, OLF, and YRK, while regressions of OC to $PM_{2.5}$ produced r^2 = 0.56, 0.70, and 0.71. Performing the same correlation studies using the 60-min resolution from the continuous $PM_{2.5}$ mass and chemistry measurements from the SEARCH sites produced similar numbers for r^2: 0.27, 0.54, and 0.59 for SO_4^{2-}: CTR, OLF, and YRK and 0.82, 0.54, and 0.66 for OC: CTR, OLF, and YRK, respectively.

Sulfate and organic aerosol mass did experience diurnal variability, as seen in Figure S1, with sulfate peaking around noon local time (LT) and reaching a minimum between 3 and 6 AM LT, with an average 24-hr variability of 18%, 31%, and 19% at the CTR, OLF, and YRK sites (the UAH site did not have hourly speciation available). Similarly, OC peaked compared to its 24-hr mean by 22%, 26%, and 17% at CTR, OLF, and YRK, on average. Contrary to the SO_4^{2-} mass, the OC mass would peak before sunrise and the total $PM_{2.5}$ mass would peak in the early morning hours, varying by 21%, 33%, and 16% on average during the day at CTR, OLF, and YRK, respectively, causing variations in the SO_4:OC ratio as large as 30% within 24 hr. This variability may be due to differing source contributions (e.g., local traffic in the morning at the UAH and OLF sites) but a more probable scenario is the development of an aerosol reservoir aloft in the nighttime PBL residual layer. Daytime convection then brings this sulfate back down to the surface as it would for the cloud processed aerosol particles for the remainder of the day.

3.2. Light Scattering Coefficients and Mass Scattering Efficiency

Time series of daily-averaged surface aerosol optical properties are presented in Figure 5. Dry particle light scattering coefficients (σ_{sp}) at 550 nm ranged from 5 to 125/Mm, with correlations between sites on par with $PM_{2.5}$. Dry light scattering and $PM_{2.5}$ were tightly correlated at each site (Figure 6a), although OLF had a markedly lower slope consistent with the higher dust mass fractions. Particle mass scattering efficiency (α_{sp}) can be calculated in two different manners. More commonly, α_{sp} is simply the mean σ_{sp} divided by the mean $PM_{2.5}$ mass. Alternatively, the slope of the σ_{sp} to $PM_{2.5}$ regression yields a specific mass scattering efficiency ($\alpha_{sp,spec}$). These values more likely capture the sensitivities of the dominant aerosol species σ_{sp} (here FM) to changes in mass while minimizing the effect of non or random variant species, such as background coarse mode particles captured below the 2.5 μm diameter cut point. The regression is the best overall linear predictor of $\alpha_{sp,spec}$ from $PM_{2.5}$. This said, there is clear nonlinearity in the data points relative to the regression line.

Mean values of α_{sp} were 3.7, 2.3, and 3.6 m^2/g for CTR, OLF, and YRK, respectively. These numbers are more representative of bulk properties of an equally weighted sample. There was ~33% variability in α_{sp} at each site on a day-to-day basis (Figure 5b), and some correlation existed between the CTR and YRK sites (r^2 = 0.34). The regression derived values $\alpha_{sp,spec}$ were slightly higher at 4.5, 2.6, and 4.7 m^2/g at CTR, OLF, and YRK, respectively (Table 2). In all cases OLF had markedly lower values of α_{sp}, although the exact reason is unclear. Background coarse mode mass that intrudes beyond the $PM_{2.5}$ cut point would drive the values downwards for OLF, especially for low background pollution concentrations and for dust intrusions. Sea salt did not appear as a major player and, as will be shown later, AERONET r_{eff} retrievals at OLF were only slightly smaller than at the other sites.

Diurnal variations in α_{sp} were minimal, varying as little as 18%, 14%, and 12% at CTR, OLF, and YRK, respectively, peaking overnight and in the early morning hours, corresponding to peaks in $PM_{2.5}$ mass. However, the α_{sp} peaks in around noon LT, roughly corresponding to peaks in the SO_4:OC ratio, although it would also experience a smaller peak overnight, when the SO_4:OC ratio was at a minimum.

The α_{sp} are dependent on particle refractive index, particle density, aerosol size distribution (e.g., Malm & Hand, 2007; Reid et al., 1998). All three of these variables are influenced by aerosol chemistry, creating a complex nonlinear system that has remained difficult to characterize theoretically. Our bulk findings are consistent with this. Comparison of the σ_{sp} and α_{sp} shows some covariance, and α_{sp} systematically increases with higher $PM_{2.5}$ (Figure 6b) as has been observed previously (Malm & Hand, 2007). This would suggest that for more significant haze events, the aerosol population has an increase in FM size and/or index of refraction. There was, however, virtually no relationship between α_{sp} and the measured SO_4:OC ratio. The only reasonable assessment then is size or refractive index, or an increased influence on mass of particle-bound water on the collection filters.

The findings here are nominally in agreement with the literature review by Hand and Malm (2007) that yielded an average α_{sp} of 3.4 ± 1.2 m^2/g, for $PM_{2.5}$. They noted a higher urban mean α_{sp} at 5 m^2/g and

rural mean α_{sp} approaching the theoretical scattering efficiency of dry ammonium sulfate at 2.5 m^2/g. Here we find the higher values indicative of more polluted rural conditions, at the CTR and YRK sites, while the lower value at the OLF site approaches the "clean rural" conditions described in the literature.

3.3. Light Absorption and Extinction

While there was some variability in α_{sp} between sites, σ_{ap} was much more regionally similar. From section 3.1, BC was moderately well correlated with the CTR site (Figure 3e). Likewise the light absorption coefficient (σ_{ap}) was consistent among SEARCH sites, both against $PM_{2.5}$ and BC (Figures 6d and 6e). This said, at the UAH site, BC mass fractions were markedly lower than at SEARCH sites (Figure 4d), but unfortunately, no absorption measurements were available.

The mass absorption efficiency (α_{ap}) is dependent primarily upon BC concentrations within the aerosol, with some contribution from brown carbon and dust (White et al., 2016). With fairly constant BC mass concentrations at all sites, the observed absorption coefficients (σ_{ap}) were similar across the three sites with 24-hr means at 5/Mm, producing similar mean bulk α_{ap} of 0.6–0.7 m^2/g (Figures 5c and 6d) Using the regression method did not significantly change the α_{ap} results, and there was no significant change observed with an increase in $PM_{2.5}$ mass nor SO_4:OC ratios with the exception of the OLF α_{ap} (Figures 6f and 6g), but even this is not statistically significant. Nevertheless, the α_{ap} regression against thermal BC was stable, ranging from 10.5 to 13.4 m^2/g, on the higher side of accepted values (Bond et al., 2013). One noticeable trend was an increase in α_{ap} starting in late September (Figure 6c), consistent with an increase in BC mass and mass fraction (Figures 3e and 4d) and coincided with more fall like weather, likely due to an increase in wood-burning stoves (Zheng et al., 2002). Similar to σ_{sp}, σ_{ap} experienced diurnal variations of 24–34%, peaking around noon LT with a secondary peak overnight compared to the 24-hr mean.

Summing α_{sp} and α_{ap} yields the mass extinction efficiency (α_{ext}). As expected α_{ext} was lowest at the OLF site, at 2.9 ± 0.6 m^2/g, and was identical at the CTR and YRK sites with means and standard deviations of 4.2 ± 0.8 m^2/g. Unlike α_{sp}, α_{ap} appeared insensitive to $PM_{2.5}$ (Figure 6f), yet α_{sp} did drive a slight increase in α_{ext} with $PM_{2.5}$.

Finally, we consider single-scattering albedo (ω_o), which can be derived by point average and regression. Overall, σ_{sp} and σ_{ext} were tightly correlated (Figure 6h), yielding mean dry ω_o values of 0.85–0.86 for CTR and YRK and excellent intercorrelations between them (Figure 5d). However, OLF was markedly lower at 0.77, a result of lower α_{sp} relative to other sites than α_{ap}. In general, ω_o was lower and noisier for lower $PM_{2.5}$, consistent with the tendency for α_{sp} although all sites converged to 0.90 for higher aerosol $PM_{2.5}$ concentrations (Figure 6i). With an increase in BC mass fraction and α_{ap}, ω_o also dropped in the fall (Figure 5d).

3.4. AERONET

From ground-based aerosol optical properties, we proceed to AERONET AOD measurements and inverted properties. For a possible 153 days of data, AERONET sites provided 64–103 data days, or nominally a 42–67% yield. Lower yield sites, like OLF and YRK, suffered from several data outages during the study. We estimate total daily cloud cover resulted in a 40% loss of data. AERONET-derived properties are presented in Figure 7 and Table 3. AOD generally tracked $PM_{2.5}$ events with a mean value and standard deviations of AERONET-derived 550 nm AODs for the four sites (CTR, OLF, YRK, and UAH) of 0.17 ± 0.10, 0.16 ± 0.11, 0.16 ± 0.11, and 0.16 ± 0.10, respectively. AODs were reasonably well correlated between sites (e.g., Figure 7a), but interestingly not as well as $PM_{2.5}$ (Figure 3a). Autocorrelation analysis also showed that while $PM_{2.5}$ had an *e*-folding correlation of 3 days at each site, for AOD, it dropped to one day. This behavior is due in part to a noncontiguous data set in AOD due to data outages and cloud cover, but even when one-day gaps are replaced with linear correlations between days, the results are nearly the same. Indeed, it is clear from Figure 7 that strong single-day spikes in AOD are far more prevalent than in $PM_{2.5}$. Thus, it is quite likely that the autocorrelation lengths and times for surface $PM_{2.5}$ over the SEUS region are larger than AOD counterparts. This is partially apparent in the example of 9 September presented in Figure 1f where large AOD halos exist around areas of convection. One outlier in the regression was also observed, a very high AOD at OLF relative to other sites on 12 September. Satellite imagery showed significant prescribed biomass burning in the area on this day and is removed in subsequent analysis. Also notable is the precipitous drop in AOD over the region after 20 September with the change to more fall-like weather. During daylight hours, AOD values varied by 25% on average, peaking around 10 am LT, coincidental to peaks in $PM_{2.5}$ mass.

Table 3
Number of Measurements (N), Means, and Standard Deviations for AERONET and Satellite Products

	CTR	OLF	YRK	UAH
AERONET properties				
N measurements	112	97	79	93
AOD-550 nm	0.17 ± 0.10	0.16 ± 0.11	0.16 ± 0.11	0.16 ± 0.10
10th/90th% AOD	0.06/0.32	0.06/0.28	0.06/0.28	0.06/0.30
AOD min/max	0.02/0.5	0.03/0.64	0.03/0.64	0.02/0.53
FMF-550 nm	0.80 ± 0.10	0.68 ± 0.19	0.86 ± 0.13	0.90 ± 0.09
Angstrom exp. 440–870 nm	1.6 ± 0.3	1.2 ± 0.4	1.7 ± 0.3	1.7 ± 0.2
FM eff. radius, μm	0.16 ± 0.02	0.15 ± 0.02	0.15 ± 0.01	0.16 ± 0.02
Refr. index (440 nm): real	9: 1.4 ± 0.04	8: 1.4 ± 0.04	1: 1.4	8: 1.4 ± 0.03
Refr. index (440 nm): imag	0.004i ± 0.002i	0.005i ± 0.001i	0.01i	0.01i ± 0.005i
Satellite AOD N: Avg ± Stdev				
Terra MODIS 550 nm	55: 0.21 ± 0.15	40: 0.19 ± 0.14	50: 0.18 ± 0.14	53: 0.18 ± 0.13
Aqua MODIS 550 nm	36: 0.14 ± 0.11	35: 0.16 ± 0.13	27: 0.12 ± 0.12	38: 0.18 ± 0.13
Terra MISR 558 nm	6: 0.10 ± 0.07	10: 0.15 ± 0.12	8: 0.15 ± 0.12	14: 0.17 ± 0.08

Note. The refractive index (Refr. index) is broken into real and imaginary components. Refractive index and satellite AOD statistics include the number of measurements (N: Avg ± Stdev). FMF is the fine mode fraction AOD, and FM eff. radius is the Dubovik-derived fine mode effective radius.

Unsurprisingly, as all sites had a mean $PM_{2.5}$:PM_{10} value of 0.6, AOD was dominated by FM aerosol particles (Figure 7b). The SDA+ estimates of FM fraction ranged from 0.68 at OLF to 0.90 at UAH (Table 3)—consistent with OLF's lower mass scattering efficiency. Coarse mode AOD means were 0.02–0.06 at each site with the OLF site having the highest value, perhaps due to the location's dust influence or marine influence—although as we noted the sea salt mass fractions were low within the surface-level $PM_{2.5}$ aerosol mass. Nevertheless, marine influence could extend above the local boundary layer, or as mentioned earlier, masked by Cl^- depletion. Occasional perturbations in CM AOD in the 0.05–0.2 range were visible at OLF and CTR, likely the result of aforementioned African dust represented in the soil times series, or biomass burning. The CM AOD peaks in June match dust measurements at the sites (e.g., Figure 3d).

Ångström exponents (Ångström, 1929) were calculated as $-\log(\tau_{\lambda,1}/\tau_{\lambda,2})/\log(\lambda_1/\lambda_2)$, where $\tau_{\lambda,1}/\tau_{\lambda,2}$ is the ratio of the AOD at two wavelengths, λ_1 and λ_2. Using τ at 440 and 870 nm, Ångström exponents were consistent with the dominant FM fraction, ranging from 1.2 to 1.7, and had slight correlations between sites (Figure 7d). Examining Dubovik retrievals for FM effective radius for all retrievals where 440 nm AOD $>$ 0.1, column integrated sizes were remarkably stable and mean r_{eff} from 0.15 to 0.16 μm for all sites, with standard deviations on the order of 0.01–0.02.

AERONET inversions are also able to provide estimates of refractive index and subsequently derived ω_o and on a subset of days when AERONET 440 nm AOD is greater than 0.4 (N = 9, 8, 1, and 8 for CTR, OLF, YRK, and UAH; Table 3). This limited the number of cases available that fit these criteria, coupled with the lack of a retrieval at 550 nm, and the ambient column-averaged RH makes direct comparisons between AERONET and dry, surface-based ω_o observations useless. With the caveat that the nephelometer ω_o is representative of dry, surface-level aerosols and the AERONET-derived aerosols are measurements of column-averaged aerosols at ambient RH, we can make some observations. Even without direct comparison, we can note that overall the AERONET-derived ω_o are higher than the dry, surface-level ω_o (0.97, 0.96, 0.96, and 0.96 for CTR, OLF, YRK, and UAH, respectively; Table 3). AERONET-derived ω_o is not necessarily representative of steady state ω_o as they can only be observed during high-pollution events. The mean AERONET-derived ω_o when AOD $>$ 0.4 (a necessary condition for derivation) are CTR: 0.90 ± 0.02; OLF: 0.83 ± 0.02 YRK: 0.85, and CTR: 0.85 ± 0.05, OLF: 0.76 ± 0.06, YRK: 0.85 ± 0.05, greater than the mean surface-level ω_o observed at these sites. The YRK site had only one comparable AOD and no standard deviation during the SEAC^{4}RS time period. With the other two sites we can clearly see that the high AOD days necessary for the derivation of AERONET-derived ω_o create artificially high ω_o. This is likely due to the change of the α_{sp} during high pollution events discussed in the previous section, whereas α_{ap} either has no dependence or a weak negative dependence on $PM_{2.5}$ mass, or an increase in RH during high pollution events. A comparison of the refractive indices across

Table 4
Agreement of Both Fine Mode AERONET (FM AERO) and Satellite AODs Relative to 24 hr and 60-min Average Total 550 nm AERONET AOD

	CTR (r^2/RMSE/bias)	OLF (r^2/RMSE/bias)	YRK (r^2/RMSE/bias)	UAH (r^2/RMSE/bias)
AERONET 550 nm AOD: 24-hr mean				
FM AERO.	0.93/0.04/0.03	0.92/0.06/−0.06	0.95/0.04/−0.3	0.96/0.03/−0.03
T. MODIS AOD	0.46/0.09/−0.01	0.87/0.06/−0.03	0.87/0.07/−0.02	0.82/0.06/−0.01
A. MODIS AOD	0.87/0.06/−0.04	0.86/0.06/0.03	0.90/0.08/−0.05	0.86/0.00/−0.02
T. MISR AOD	0.92/0.09/0.07	0.76/0.08/0.06	0.99/0.03/0.02	0.94/0.02/0.02
AERONET 550 nm AOD: 60-min mean				
T. MODIS AOD	0.81/0.08/−0.04	0.63/0.01/−0.01	0.64/0.03/0.0	0.35/0.06/0.01
A. MODIS AOD	0.80/0.08/−0.05	0.32/0.01/−0.01	0.33/0.07/−0.04	0.29/0.05/−0.01
T. MISR AOD	0.91/0.07/0.05	0.34/N/A/N/A	0.92/0.01/0.0	0.98/0.04/0.0

Note. The satellite instruments used in this study include the Terra MODIS (T. MODIS), Aqua MODIS (A. MODIS), and the Terra MISR (T. MISR). All AODs are reported at the 550 nm wavelength, except the Terra MISR measurement, which was made at the 558 nm wavelength. The 60-min mean was calculated on the hour.

the sites reveals that they are consistent across the sites with values at 1.4 + 0.01i, consistent with the sites consisting of hygroscopic aerosols heavily influenced by water (Liu & Daum, 2000). Thus, while we cannot say that the AERONET retrieval is verified, it is nevertheless within reasonable expected bounds for high pollution days in a humid environment.

3.5. Satellite AOD

To assess satellite AOD data quality at each site, Terra and Aqua MODIS and Terra MISR AODs were extracted for each grid proximate to the sites under investigation here. Statistics and regressions with AERONET AOD are provided in Tables 3 and 4. As noted in section 2, individual retrievals were within 0.3° of the site. The temporal differences between AERONET observations and satellite overpasses are chosen to be within ±30 min, following a few previous studies (e.g., Petrenko et al., 2012; Shi et al., 2011). MODIS-derived mission average and standard deviation AOD converged to AERONET values. MISR, however, showed a significant low bias to the AERONET average values. As discussed below, this appears to be related to an overall low bias in AOD coupled with infrequent sampling.

Regressions were performed between MODIS and MISR-retrieved AOD to the total AERONET AOD (Figure 8 and Table 4). For consistency we use the daily average AERONET values, although as discussed in the next section comparisons of ±30 min yielded nearly identical results. Overall there was wide-ranging correlation between the satellite and AERONET AODs, ranging from r^2 = 0.46 to 0.99. Terra MODIS retrievals were the most consistent of sensors with the highest correlations, but had high biases relative to AERONET, on the order of 10–30% at each site (Figure 8a). Aqua MODIS AODs also correlated relatively well but had more scatter and was slightly lower biased relative to Terra. Agreement between MODIS and AERONET average AODs is in part due to sampling, with unavailable retrieval days having a proclivity for lower AODs. MISR showed excellent correlations to AERONET (r^2 = 0.76–0.99), but a pronounced low bias on the order of 30%, although this can also be due to the small number of MISR observations. This low bias, coupled with few available observations due to sensor width, resulted in a significant low bias in the seasonal average AOD over the region.

3.6. $PM_{2.5}$-AOD Relationships

We briefly present the $PM_{2.5}$ to AOD regression results to assess whether AOD data were representative of $PM_{2.5}$. Figure 9 provides scatter plots of $PM_{2.5}$ to (a) AERONET 550 nm AOD, (b) Terra MODIS 550 nm AOD, (c) Aqua MODIS 550 nm AOD, and (d) MISR 558 nm AOD. As expected, AERONET values correlated the best overall with r^2 from a low of 0.36 for CTR, to a high of 0.53 at YRK. AERONET AOD-$PM_{2.5}$ *y*-intercepts, which could be interpreted as background surface values, were remarkably consistent between SEARCH sites, at ~5 $\mu g/m^3$, and only slightly higher at ~8 $\mu g/m^3$ for UAH. Slopes bifurcated strongly between sites with UAH and YRK in the northern part of the domain at ~30 $\mu g \cdot m^{-3} \cdot AOD^{-1}$ and CTR and OLF in the south at ~21 $\mu g/m^3$. Moving from AERONET to MODIS-derived AODs (Figures 9b and 9c), correlations somewhat decreased, but more dramatically were changes in slopes, reflecting not only biases in AOD (e.g., section 3.5) but also sampling. The sampling issue is acute for MISR (Figure 9d), with both regression r^2

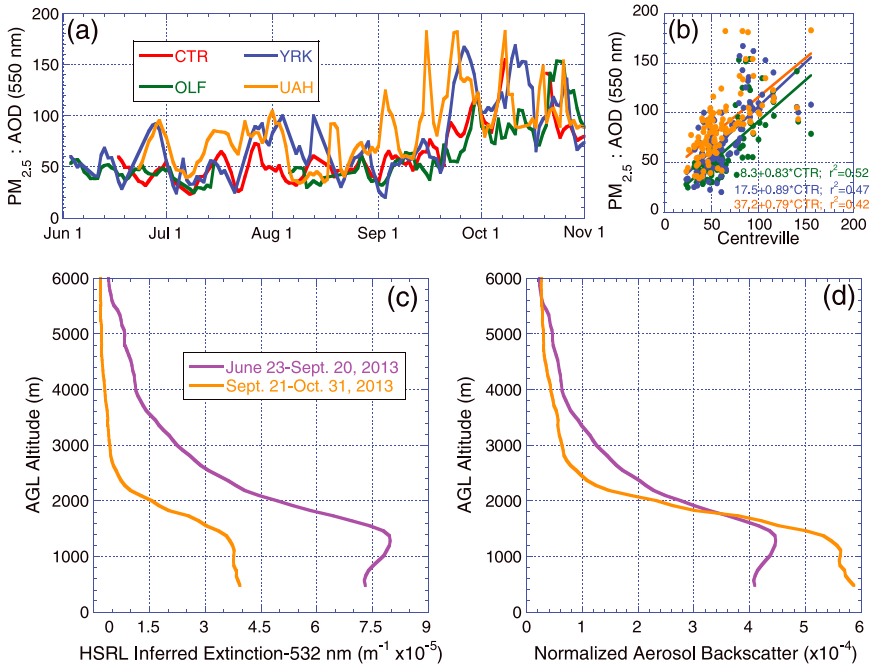

Figure 10. Influence of seasonality on the $PM_{2.5}$ to AOD relationship including (a) time series of the five-day boxcar average ratio of $PM_{2.5}$ to AERONET 550 nm AOD; (b) the $PM_{2.5}$ to AOD ratio between sites, including linear regression statistics; (c) the average UAH HSRL inferred extinction distribution for cloud free cases for the summer and autumnal time period; and (d) backscatter profiles normalized to total integrated backscatter.

and slopes and *y*-intercepts highly variable based on the influence of one or two points. Theil regressions were also performed so as to reduce the influence of outlying values, and yielded similar results, with slopes/intercepts of 20/5.6, 23/4.9, 28/5.7, and 36/4.7 for the AERONET-$PM_{2.5}$ relationship; 20/6.0, 18/6.5, 21/6.2, and 34/4.8 for the Terra MODIS-$PM_{2.5}$ relationship; and 20/3.9, 11/8.0, 36/4.2, and 62/1.8 for the Terra MISR-$PM_{2.5}$ relationship at CTR, OLF, YRK, and UAH, respectively.

Due to the diurnal variations in both $PM_{2.5}$ mass and AODs, the question arises if the linear agreement can be improved using 60-min averages rather than 24-hr averages of the measurements, particularly as the satellite-derived AOD values represent a single point in time and the AERONET AOD values are limited to daylight hours. However, the regression statistics in Table S1 show only marginal improvement in agreement at some sites, and marked deterioration at other sites, ultimately revealing no clear trend.

The results from the regression of $PM_{2.5}$ to AOD are largely related to the vertical profile of aerosol particles and their hygroscopicity. Within the PBL, RH generally increases with height. Hygroscopic aerosols grow with increasing RH due to the adsorption of water, increasing light scattering and backscatter. This can be seen in the lidar profiles obtained during the SEAC^{4}RS campaign at UAH. Examination of the data showed that the $PM_{2.5}$ to AOD ratio had strong seasonality (Figure 10a), changing around 20 September 2013 when the overall meteorology shifted from summer convective to autumn frontal behavior. Figure 10a provides the time series of the five-day boxcar average ratio of $PM_{2.5}$ to AERONET 550 nm AOD. Throughout the summer the bulk ratios were similar across all sites at ~50 $\mu g \cdot m^{-3} \cdot AOD^{-1}$. The ratio in general correlated between sites generally well (Figure 10b), but clearly in mid-to-late September the ratio increased substantially. We surmise that this is largely due to changes in the aerosol vertical distribution. Figure 11c provides the average UAH HSRL inferred extinction distribution for cloud free cases taken from Reid et al. (2017). The summer and fall periods are delineated by 20 September 2012. Extinction is here calculated assuming a uniform lidar ratio of 55 str as used by Reid et al. (2017). As expected, extinction is higher in the summer months commensurate with higher AOD. Aerosol extinction was dominated by the PBL mixed layer near the surface, and sloping off monotonically to the midfree troposphere with layers there being largely associated with either a deep PBL entrainment zone, convective lofting to the free troposphere, or the long-range transport of smoke from the western United States. If we normalize these profiles to total integrated backscatter (Figure 10d), we clearly

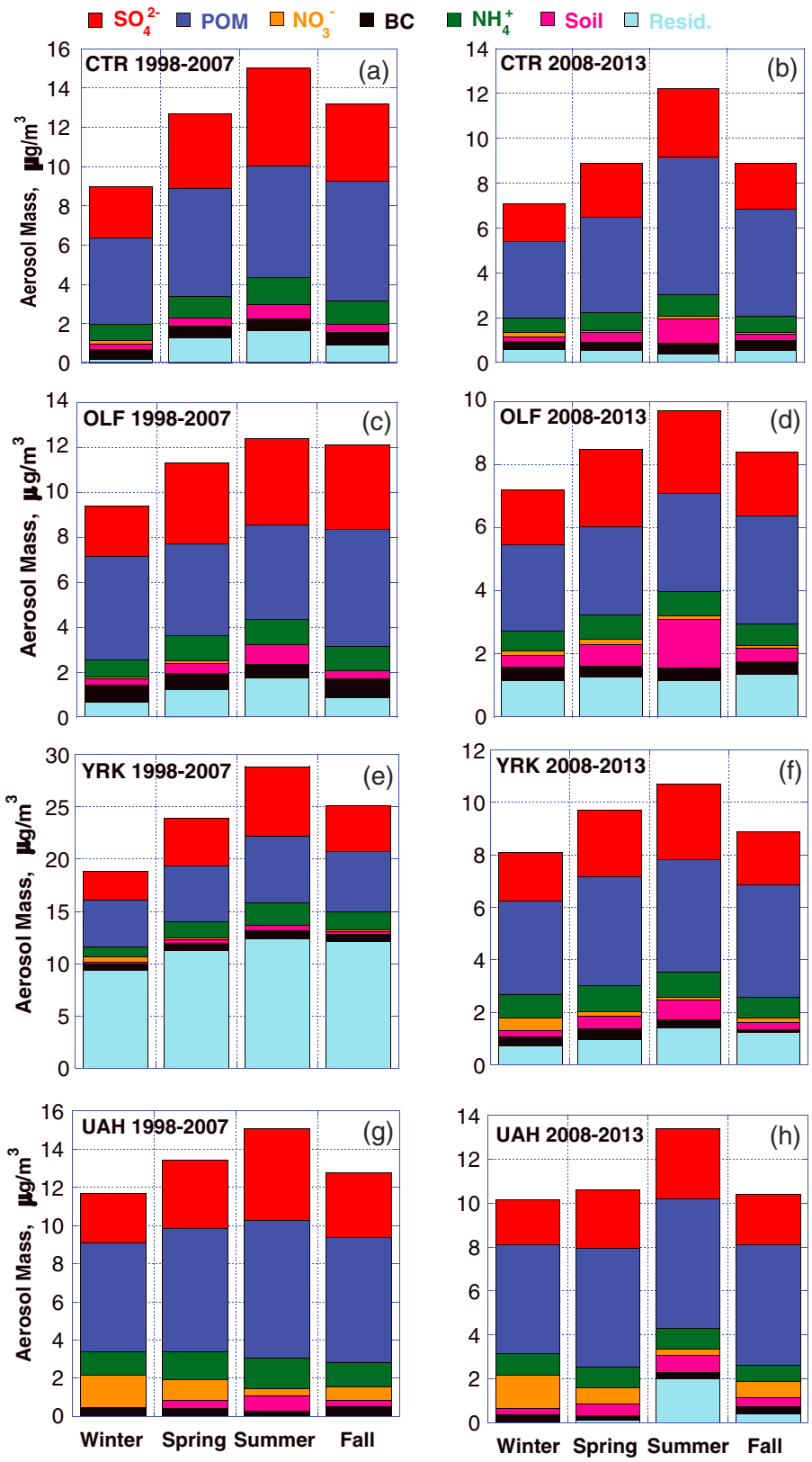

Figure 11. Dry aerosol mass seasonal averages for (a, c, e, and g) the 1998–2007 period and (b, d, g, and h) the 2008–2013 period for the SEARCH/SEAC^{4}RS sites. Chemistry reported include particulate organic matter (POM, defined as 1.8*organic carbon mass), black carbon (BC), and filter mass residual (resid.).

see significant changes in profile shape between the summer and autumn regimes. Near the surface in the summer months, there is a peak in extinction at the top of a well-developed mixed layer at ~1.2 km. This is due to the presence of a typically well-mixed mixed-layer, with hygroscopicity increasing extinction as the RH increases with altitude. Fall-like conditions, however, showed more uniform extinction profile due to the formation of low-level surface layers in the nighttime and morning hours during cooler fall (Reid et al., 2017). Above the mixed layer summertime extinction subsequently falls off more slowly than its autumn counterpart owing to a deep convective entrainment zone as well as the transport of biomass burning smoke from the Pacific Northwest (Reid et al., 2017).

The variability in the ratio of $PM_{2.5}$ to AOD is not entirely due to vertical distribution. Comparison of AERONET AOD to integrated backscatter suggests that during the autumn months, a lidar ratio of 48 str is more appropriate than the baseline value of 55 str used here. This decrease in lidar ratio can be a result of changes in chemistry but also in size. Indeed, based on previous subsections, retrieved r_{eff} dropped in the autumn period and the organic mass fraction increased. Both of these might lead to a decrease in lidar ratio and mass scattering efficiency.

4. Results II: Representativeness, Intercorrelation, and Perspective

While the scope of the SEAC^{4}RS campaign was extensive, and the data analysis, performed both here and elsewhere (e.g., Attwood et al., 2014; Brock, Wagner, Anderson, Attwood et al., 2016; Brock, Wagner, Anderson, Beyersdorf et al., 2016; Reid et al., 2017), has been thorough, we also must examine the data within the climate perspective. In the following sections we put the data in the context of both seasonal variability and annual long-term trends, and analyze the geographic relationships of site-specific data. We investigate the temporal variability of the $PM_{2.5}$-AOD relationship and identify potential issues. Finally we compare the ability of using site intercorrelations to predict $PM_{2.5}$ and compare the results to using AOD measurements to predict $PM_{2.5}$.

4.1. Representativeness to Long-Term Regional Aerosol Properties

As the combined 2013 field campaigns were limited to a five-month span, there is the question as to how representative temporally the results from these five months are to the region as a whole. Fortunately, the CSN site at the UAH location, and the SEARCH sites at CTR, OLF, and YRK span a period dating from 1998 through 2015 at the SEARCH sites, and 1999 through 2015 for the CSN site. The SEARCH nephelometer data were only available from 2007 through 2014 and the aethelometer data collection began 2008. The SEARCH AERONET sites collected data from 2013 onward, while the UAH site collected AERONET-derived AODs from 2008, but is subject to large periods of outage. Satellite-derived AOD measurements are available for the site beginning in 2000 for the Terra instruments and 2002 for the Aqua instrument.

To examine how the SEAC^{4}RS results fit into the larger picture, first we look at seasonal differences to investigate how SEAC^{4}RS was representative of typical seasonal behavior. Then we examine the representativeness of 2013 in the long-term trends.

4.1.1. Seasonal Variability

Seasonal variations have a large impact on observed aerosol variations for the SEUS region (Figure 11 and Table S2). For the following analysis we extend the data from 2013 to 2015, when available, to better capture seasonal trends, particularly in the AERONET AOD as the SEARCH AERONET sites were not established until summer 2013. Section 4.1.2 will examine seasonal trends dating back to 1997. Seasons are defined as winter (December–February), spring (March–May), summer (June–August), and fall (September–November).

Large seasonal variations in aerosol chemistry and optical properties are observed, consistent with previously published papers (e.g., Hand et al., 2012). $PM_{2.5}$ concentrations are lowest in the winter, reflecting a decrease in both primary sources and optimal conditions for secondary pathways. The exception to this in nitrate, which peaks in the winter at all sites as its formation pathway is optimized by the low temperatures and high RHs experienced by winters, but most noticeably at the urban UAH site, with nitrate ion composing 20% of the $PM_{2.5}$ mass in the winter mean of 2013–2015. BC also has a smaller peak in relative and absolute concentrations in the fall and winter, which has been previously sourced to an increase in wood-fire burning in the cold-weather months (Zheng et al., 2002).

As observed in previously published work (Ford & Heald, 2013; Hand et al., 2013) the OC component demonstrates seasonal differences, with a drop in absolute OC mass of 32%, 7%, 29%, and 32% at the CTR, OLF, YRK, and UAH sites in the winter months compared to the summer months, primarily attributed to differences in primary biogenic volatile organic carbon emissions. While Table S2 shows an increase in the relative mass concentration of OC in the fall months compared to the summer months, this is due to a decrease in total aerosol mass, not an increase in absolute OC mass. Similarly, SO_4^{2-} concentrations peaked in the summer months by 0.3, 0.4, 0.6, and 0.4 $\mu g/m^3$ relative to the winter months for CTR, OLF, YRK, and UAH, respectively. The soil/dust also increased in the summer with an increase in agricultural activity, biomass burnings, and long-distance advection of African dust (Hand et al., 2017; Xian et al., 2016), driving a dip in the $PM_{2.5}$:PM_{10} ratio.

The seasonal variations observed in the satellite-derived AODs as well as the AERONET AODs (Table S3) reflect the variations in $PM_{2.5}$ mass, with AODs peaking in the summer months by as much as 400% compared to the winter months, similar to what has been observed previously (e.g., Alston et al., 2012). The reason for the greater seasonable variability in the AODs relative to surface $PM_{2.5}$ mass is still being debated with potential solutions including an unresolved upper atmospheric OC layer and a summertime increase in the atmospheric water column (Ford & Heald, 2013; Nguyen et al., 2016; Reid et al., 2017). The dry aerosol scattering coefficients follow predictable patterns, peaking at summer when aerosol mass and AERONET retrieved size peaks, and plummeting in the winter. Similarly, the CTR and OLF absorption coefficients increase in the fall, following BC trends.

The α_{sp} and α_{ap} vary by ~10% at all sites (Table S3), peaking in the summer with sulfate concentrations, with the exception of the OLF site, whose mean α_{sp} is consistently less than the CTR and YRK sites, and show no seasonal pattern. Other monitoring sites have recorded an increase in α_{sp} coincident with an increase in $PM_{2.5}$ mass, possibly due to the aging processes under polluted conditions, shifting the particle distributions to larger sizes (Lowenthal & Kumar, 2004). The CTR and YRK sites are consistent with this.

The seasonal differences observed in the $PM_{2.5}$ and AOD coupled with changes in environmental conditions impact their linear relationship. Examining the 2013–2015 means, the winter season demonstrated the highest $PM_{2.5}$-AOD regression coefficient, with slopes of 48, 57, 37, and 48 $\mu g/m^3$, with r^2 values of 0.27, 0.14, 0.13, and 0.27 at CTR, OLF, YRK, and UAH, respectively. This compares to low summertime regression coefficients of 22, 20, 18, and 23, with r^2 values of 0.27, 0.34, 0.22, and 0.31 at CTR, OLF, YRK, and UAH. The smaller slopes in the summertime could be a result of the higher dry α_{sp}, changes in aerosol hygroscopicity due to changes in chemistry, and higher mixed layer height. The intercepts at all sites and all seasons ranged from 4 to 9 $\mu g/m^3$, with winter exhibiting the smallest intercepts of 4 to 6 $\mu g/m^3$.

4.1.2. Long-Term and Seasonal Trends

The SEARCH sites offer 17 years of surface observations and the UAH CSN site provides 12 years of observations, which serve to put the 2013 missions in perspective in regard to longer-term trends. Filter collection and analysis of aerosols began in 1998 at the CTR and YRK sites and 1999 at the OLF site. While the UAH CSN site performed gravimetric analysis starting at 1999, chemical analysis of the aerosols was not recorded until 2003. The representativeness of 2013 annual averages compared to the longer term is shown in Figure 12 and Table S4. The long-term trends are further broken up into the period prior to 2008, and the period post-2008, as clean-power plant regulations went into effect in 2008, compounded by the impacts of a recession, and caused significant changes in aerosol mass, aerosol composition, optical depth and potentially forcing (Brewer et al., 2014; Hand et al., 2012, 2014; Tosca et al., 2017).

A downward trend in the aerosol mass can be observed in Figure 12a, with the largest decline in $PM_{2.5}$ mass occurring after the clean power plan regulations in 2008, with the 2008–2013 period $PM_{2.5}$ experiencing a decrease of 30%, 25%, 30%, and 24% in mean aerosol mass for CTR, OLF, YRK, and UAH, respectively, compared to the 1997–2007 period. Furthermore, the mean annual $PM_{2.5}$ mass recorded for 2013 decreased by 12%, 10%, 12%, and 21%, for CTR, OLF, YRK, and UAH, respectively, from the mean over the prior five years, implying a continuing downward trend as observed in previous years (e.g., Alston et al., 2012), although consistent drops were not observed post 2013 and current regulation easements may not support further reductions in total aerosol mass (https://www.epa.gov/Energy-Independence; last viewed 28 September 17).

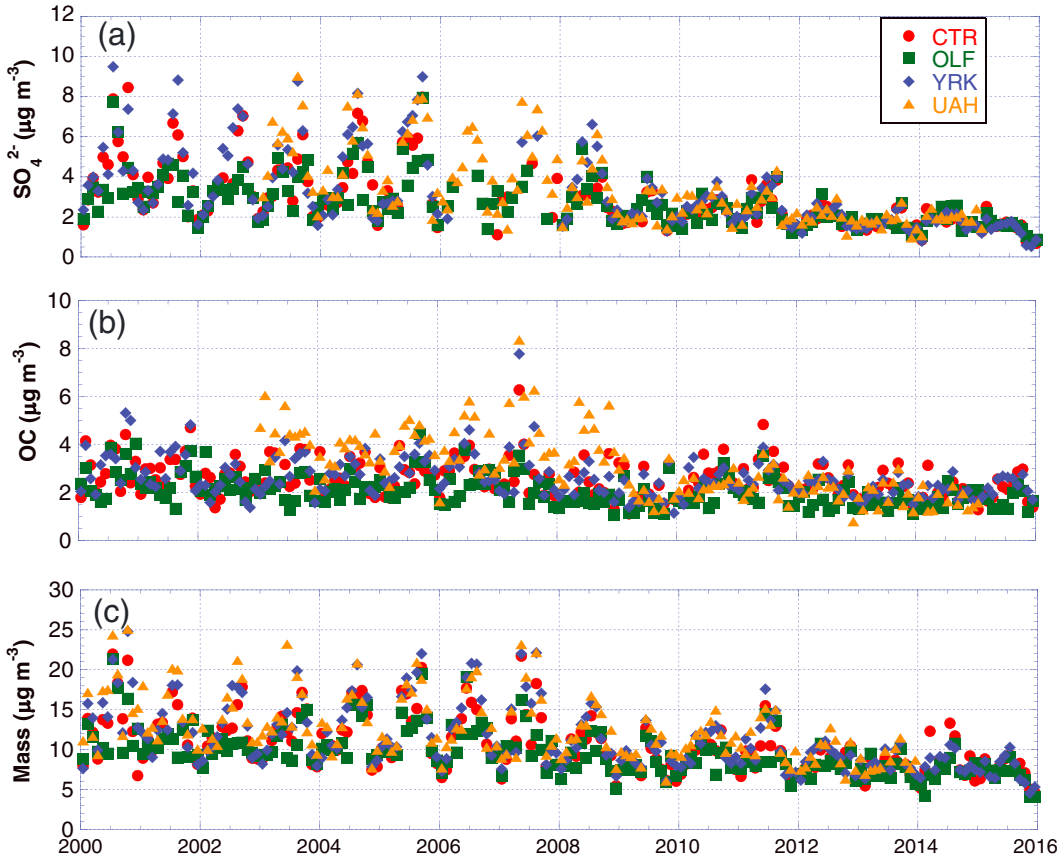

Figure 12. Monthly averaged (a) sulfate (SO_4^{2-}), (b) organic carbon (OC), and (c) $PM_{2.5}$ mass concentrations at four sites (Centreville, AL; Outlying Field, FL; Yorkville, GA; and University of Alabama Huntsville, AL).

The downward trend in $PM_{2.5}$ is accompanied by a drop in both the absolute and relative amount of sulfate aerosols at the four sites, with mass fractions in 2000–2007 of 30%, 30%, 32%, and 33% compared to 25%, 26%, 25%, and 24% in 2008–2013 at CTR, OLF, YRK, and UAH, respectively. The relative amounts of sulfate in the total aerosol mass remained about the same in 2013 and remained the same over the next two years compared to the previous five years. The OC component is slightly more difficult to characterize as changes in aerosol chemistry may change the oxidized mass associated with the OC, but a study of absolute mass shows a drop in the OC component as well, just at a rate slower than the $PM_{2.5}$, with the 2000–2007, and 2008–2013 masses of CTR 3.0 to 2.4 μg/m^3, OLF 2.5 to 1.8 μg/m^3, YRK 3.1 to 2.3 μg/m^3, and UAH 4.1 to 2.5 μg/m^3, showing either a significant drop in the anthropogenic component of the OC, or a reduced favorability of the production mechanisms of the SOA with the reduction in aerosol acidity, as seen by Malm et al. (2017). This resulted in a significant reduction in the SO_4:OC ratio, from 1.5 ± 0.7 prior to 2008 to 1.0 ± 0.7 between 2008–2013. BC experienced a similar drop of 0.3 μg/m^3 at the SEARCH sites and a smaller drop at the UAH site in the post regulatory period. The other minor aerosol chemical components had no discernable trends, with the exception of the soil/dust component, which saw a slight increase in $PM_{2.5}$ mass 2008–2013 in the rural sites and a drop at the urban UAH site, consistent with what has been previously reported in Hand et al. (2017).

All four seasons experienced a drop in $PM_{2.5}$ from the 1998–2007 period to the 2008–2013 period, as indicated in Tables S2 and S4 and Figures 11 and 12. The implementation of the 2008 regulations, compounded by the effects of the recession, had a significant reduction in the seasonal variability in the total aerosol mass as well as the sulfate component within the aerosol mass. Summer months saw the greatest reduction in aerosol mass, with seasonal differences from the winter months to the summer months dropping 6.0 μg/m^3 in 1998–2007 to 3.7 μg/m^3 in 2008-201at CTR. Similar reductions of 3.0 to 2.6 μg/m^3, 8.5 to 4.2 μg/m^3, and 7.0 to 4.4 μg/m^3 were observed at OLF, YRK, and UAH, respectively, demonstrating a

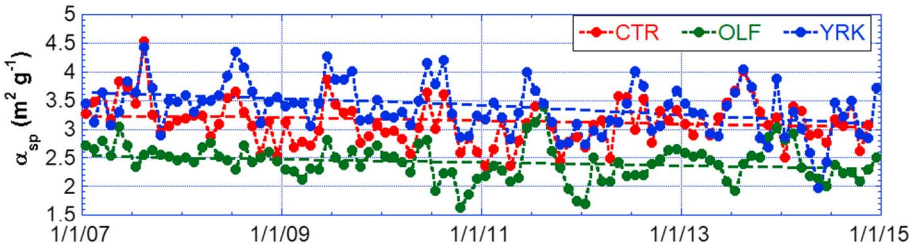

Figure 13. Monthly averaged mass scattering efficiency (αsp, λ = 530 nm) observed at the SEARCH sites, with a linear fit at every site to highlight the decrease in mass scattering efficiency with time.

significant decline in seasonal variability in SEUS aerosol mass. This decline in seasonal variability appears to be entirely due to a greater reduction of sulfate in the summer months compared to the winter months. While OC also experienced a decline in absolute mass post 2008, the reduction is more evenly distributed across the seasons. The only other aerosol component with a seasonal component between the two periods is dust, which shows a small increase in the absolute concentrations of dust at all SEARCH sites in the summer time, and an increasing relative concentration in the summer months compared to the winter months of 0.28, 0.56, and 0.32 at CTR, OLF, and YRK, respectively, consistent with what has been observed in the IMPROVE networks across the eastern U.S. (Hand et al., 2017). The UAH site showed an overall reduction in dust during all four seasons.

The impact of the large changes on aerosol chemistry, mass, and, most likely, size distributions for the two periods had a noticeable impact on the absolute dry aerosol scattering, with an annual reduction of 33%, 25%, and 35% at the CTR, OLF, and YRK sites, respectively, from 2006–2007 to 2008–2014. Long-term changes in the mass absorption and extinction efficiency are harder to characterize as the SEARCH aethelometer does not come online until 2007 and is discontinued after 2014. Figure 13 demonstrates the complexity of α_{sp}, with the monthly averages at all sites varying between 1.5 and 4 m^2/g, and every site demonstrating an overall decrease in mean α_{sp}. The YRK site α_{sp} is often slightly higher than the CTR site, and the OLF site α_{sp} is consistently lower than the other two sites. While every season at all the SEARCH sites experienced a drop in the aerosol mass scattering efficiencies (Figure 13; Tables S3 and S5), all sites saw the largest reduction between the pre-2008 period and post-2008 period in the spring months, with drops of 0.60, 0.45 and 0.13 m^2/g at CTR, OLF, and YRK, respectively, while minimal changes of 2%, 2%, and 1% at CTR, OLF, and YRK, respectively, occurred separately in fall, summer, and winter. While the decline in aerosol mass will cause a decline in aerosol scattering efficiency (Malm & Hand, 2007), no single chemical constituent can be linked to the seasonal trends, making seasonal changes in aerosol scattering efficiencies difficult to predict. While the IMPROVE program has an algorithm for predicting σ_{sp} based on the chemical constituents of the $PM_{2.5}$ (Malm & Hand, 2007), recent work found that the predictive algorithm has become less accurate, most likely due to the decline in SO_4^{2-} and POM concentrations within the $PM_{2.5}$ (J. Hand and T. Prenni, private communications, 25 June 2017).

Long-term trends of AERONET-derived AOD values are only periodically available, and only at the UAH site, which showed a small drop from 0.17 ± 0.12 to 0.14 ± 0.12 from the 2008–2013 average to the 2013 average AOD, but with the large standard deviations, it is difficult to draw conclusions from this. The SEARCH AERONET sites begin measurements in 2013 but show almost no change in the AERONET AODs measured at the SEARCH sites 2014–2015 compared to 2013. Thus, we need to turn to satellite observations.

Satellite AODs were screened for cloud fractions below 25% to limit artificially high AODs and subject to the most recent surface albedo algorithms as described by Zhang and Reid (2006). While there is disagreement among the three instruments, all averages were within one standard deviation of each other and, with the exception of the Terra MODIS measurements, all AODs showed a drop in the AODs between the 2000–2007 period and the 2008–2013 period, as well as a drop in average annual AODs in 2013 compared to the period average, of between <0.01 and 0.03. Closer analysis of the Aqua MODIS measured AODs, we see all sites experienced the largest decrease in AODs between 2000–2007 and 2008–2013 during the winter and summer months, of 39%, 23%, 27%, and 28% in the winter at CTR, OLF, YRK, and UAH, respectively, and 31%, 15%, 34%, and 29% in the summer. Similarly, the smallest decrease was demonstrated in the spring months, at 3%, 4%, 11%, and 10%, respectively.

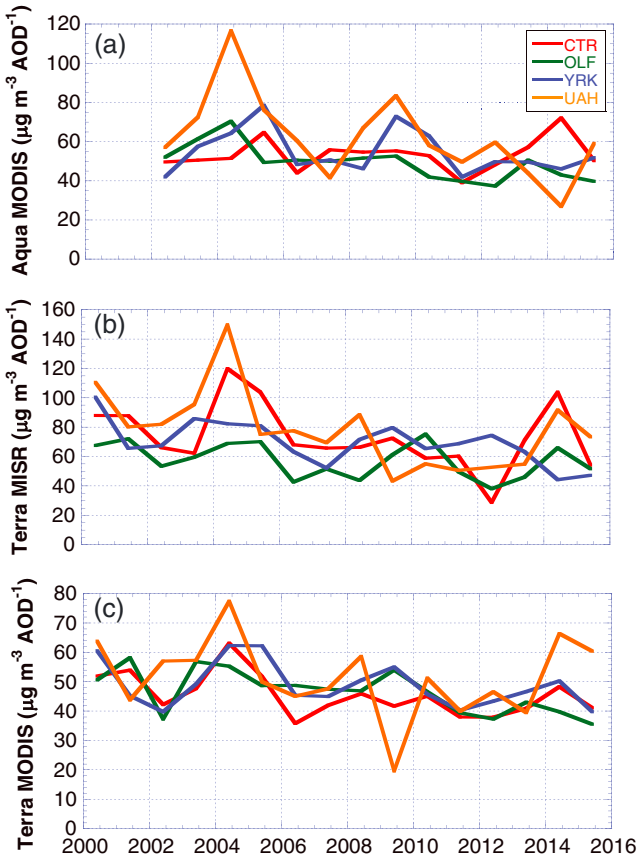

Figure 14. Annual mean $PM_{2.5}$-AOD slope at the SEARCH and UAH sites using AOD measurements from (a) the Aqua MODIS (λ = 550 nm), (b) the Terra MISR (λ = 558 nm), and (c) the Terra MODIS (λ = 550 nm). Seasonal mean $PM_{2.5}$-AOD slopes can be found in Figure S2.

The change in aerosol chemistry observed over this period is expected to impact the aerosol density, size distribution, refractive index, and hence mass scattering efficiency and hygroscopicity. These changes have a direct impact on the AOD-$PM_{2.5}$ relationship observed in section 3.6. $PM_{2.5}$-AOD regressions were calculated seasonally over a period of ~16 years and plotted in Figure 14. Overlaid are the regression coefficients calculated for annual $PM_{2.5}$-AOD observations. Table S6 includes the annual mean slope, intercept, and coefficient of determination of the historical measured ground-level $PM_{2.5}$ and satellite-derived AODs. There is an observed decrease in the annually calculated $PM_{2.5}$-AOD regression of 1 $\mu g \cdot m^{-3} \cdot AOD^{-1}$ per year at all sites between 2000 and 2015 using the Terra MODIS instrument, with coefficients of determinations of 0.27, 0.43, 0.16, and 0.03 at the CTR, OLF, YRK, and UAH sites. This could be due to the drop in aerosol scattering efficiency and a probable drop in aerosol hygroscopicity accompanying the decline in sulfate emissions, causing the AODs to be more sensitive to changes in $PM_{2.5}$ concentrations.

Strong seasonality is observed in the $PM_{2.5}$-AOD relationships, with the highest regression coefficients observed in the winter, and the lowest regressions were observed in the summer months (Figures 14 and S2) in all satellite-derived regressions. Additionally, there is a pattern of decreasing regression coefficients in both the seasonally calculated and annually calculated regressions; all seasons and all sites saw a reduction in the $PM_{2.5}$-AOD regression coefficient, although the greatest reductions in the regressions coefficients were seen in the winter months, with a drop of between 14 and 40 $\mu g \cdot m^{-3} \cdot AOD^{-1}$ in the winter months between the 2000–2007 period and the 2008–2015 period using the Terra MODIS instrument. Similarly, the summer months only experienced a drop of between 3 and 7 $\mu g \cdot m^{-3} \cdot AOD^{-1}$ at the SEARCH sites. The UAH sites actually saw a slight increase in the seasonally derived $PM_{2.5}$-AOD regression coefficients in the summer and fall months.

4.2. Intersite Correlation

As mentioned in section 3, there were varying degrees of the intercorrelation of parameters between sites. Now that a baseline of aerosol properties has been established, we will revisit the degree that properties covary between sites, with intercorrelation statistics between sites provided in Table 5. $PM_{2.5}$ was generally fair to moderately well correlate between sites. Coefficients of determinations (r^2) between the $PM_{2.5}$ at the CTR site and the other surrounding sites (~200 to 250 km apart) ranged from 0.34 to 0.63 (Figure 3). The lowest agreement among all sites arose between the geographic extremes across the domain, UAH, and the OLF at 450 km apart, with r^2 = 0.24. This is a product of both the differences in aerosol sources between a coastal rural site and an urban site, as well as their physical distance from one another. The sulfate mass were similarly correlated among the sites, with r^2 ranging between 0.2 and 0.7 for the principal chemical components of the $PM_{2.5}$ aerosols at the different sites. The soil/dust mass fractions at the three SEARCH sites were highly correlated (r^2 = 0.6–0.8), suggesting a single, long-range aerosol source or large-scale regional covariability for this aerosol component.

When extending the trend analysis to 1998–2015 for the four core sites, very little change is observed in the correlation coefficients (Table 5). Continued strong relations between the $PM_{2.5}$ mass and chemistry suggest that despite the significant changes observed in the aerosol chemistry caused by increasing $PM_{2.5}$ regulations post-2008, the aerosol mass continues to be well mixed within the region. The correlations remain strong in all four seasons, but appear the strongest in the fall months, with coefficients of determination among the $PM_{2.5}$ at all four sites ranging from 0.21 to 0.62, and weakest in the spring months, with r^2 from 0.12 to 0.45.

Table 5
Intersite Correlations Among the Four SEAC^{4}RS/SEARCH Sites

	OLF	YRK	UAH
$PM_{2.5}$ mass			
CTR $PM_{2.5}$	0.34/3.3/−0.65/0.43	0.63/2.5/0.88/0.57	0.61/2.4/1.1/0.55
OLF $PM_{2.5}$	--	0.32/3.8/1.4/0.28	0.24/3.8/1.6/0.25
YRK $PM_{2.5}$	--	--	0.74/1.9/0.47/0.63
AERONET 550 nm AOD			
CTR AERO.	0.23/0.10/−0.01/0.49	0.51/0.07/0.00/0.69	0.46/0.08/0.01/0.66
OLF AERO.	--	0.32/0.10/−0.01/0.45	0.09/0.14/0.00/0.25
YRK AERO.	--	--	0.50/0.08/0.02/0.56
$PM_{2.5}$ chemical properties			
CTR SO_4^{2-}	0.46/0.78/−0.10/0.39	0.66/0.60/0.12/0.67	0.19/0.97/0.12/0.53
OLF SO_4^{2-}	--	0.37/0.93/0.21/0.34	0.18/1.1/0.29/0.30
YRK SO_4^{2-}	--	--	0.24/0.90/−0.08/0.64
CTR OC	0.47/1.1/−0.80/0.25	0.57/0.72/−0.16/0.37	0.45/1.9/−1.8/0.45
OLF OC	--	0.25/1.0/0.61/0.11	0.30/1.3/−1.1/0.28
YRK OC	--	--	0.34/1.8/−1.6/0.51
CTR soil	0.80/1.9/1.2/0.44	0.75/0.53/0.04/0.59	0.96/0.15/−0.06/47
OLF soil	--	0.57/2.0/−1.2/0.31	0.70/2.7/−2.5/0.16
YRK soil	--	--	0.63/0.69/−0.17/0.61
CTR BC	0.50/0.13/−0.01/0.29	0.48/0.14/0.03/0.32	0.11/0.28/−0.21/0.21
OLF BC	--	0.31/0.17/−0.03/0.18	0.04/0.28/−0.21/0.33
YRK BC	--	--	0.21/0.26/−0.21/0.18
$PM_{2.5}$ optical and environmental properties			
CTR RH	0.43/7.6/3.2	0.64/5.9/2.5	0.41/12.6/−10
OLF RH	--	0.31/7.4/−0.7	0.20/16.0/−14
YRK RH	--	--	0.52/14.2/−13
CTR σ_{sp}	0.45/18/−13/0.22	0.65/11/1.9/0.34	N/A
OLF σ_{sp}	--	0.31/22/15/0.17	N/A
YRK σ_{sp}	--	--	N/A
CTR α_{sp}	0.02/1.5/−1.4/0.25	0.33/0.63/−0.15/0.42	N/A
OLF α_{sp}	--	0.0/1.5/1.2/0.34	N/A
YRK α_{sp}	--	--	N/A
CTR σ_{ap}	0.42/2.0/0.0/0.22	0.53/1.9/0.5/0.34	N/A
OLF σ_{ap}	--	0.37/2.1/0.5/0.17	N/A
YRK σ_{ap}	--	--	N/A
CTR α_{ap}	0.04/0.31/0.12/0.01	0.34/0.15/0.02/0.11	N/A
OLF α_{ap}	--	0.06/0.29/−0.09/0.04	N/A
YRK α_{ap}	--	--	N/A
CTR CM AERO.	0.53/0.03/0.02/0.38	0.36/0.02/0.00/0.40	0.37/0.02/0.00/0.51
OLF CM AERO.	--	0.24/0.04/−0.02/0.50	0.22/0.04/−0.03/0.36
YRK CM AERO.	--	--	0.23/0.02/0.00/0.36
CTR FM AERO.	0.20/0.11/−0.04/0.86	0.46/0.07/0.00/0.32	0.47/0.08/0.01/0.58
OLF FM AERO.	--	0.29/0.10/0.02/0.27	0.09/0.13/0.03/0.48
YRK FM AERO.	--	--	0.49/0.08/0.02/0.30
CTR 440–870 Ång.	0.19/0.52/−0.37/0.11	0.21/0.29/0.06/0.30	0.47/0.23/0.12/0.40
OLF 440–870 Ång.	--	0.21/0.57/0.45/0.11	0.22/0.59/0.47/0.04
YRK 440–870 Ång.	--	--	0.41/0.24/0.04/0.23
CTR FM r_{eff}	0.27/0.02/−0.01/0.29	0.32/0.01/0.00/0.32	0.59/0.01/0.00/0.43
OLF FM r_{eff}	--	0.08/0.02/0.01/0.18	0.39/0.02/0.01/0.41
YRK FM r_{eff}	--	--	0.24/0.02/0.00/0.16

Note. The first three numbers are the correlation statistics for the SEAC^{4}RS study period (r^2/RMSE/bias), and the last number is the r^2 for the measurements available for the 1998–2015 period. Dry scattering coefficients (σ_{sp}) and mass scattering efficiencies (α_{sp}) were measured at 530 nm. Dry absorption coefficients (σ_{ap}) and mass absorption efficiencies and (α_{ap}) were measured at 580 nm. The soil/dust calculation assumes the same oxides as the IMPROVE algorithm of 2.2*Al + 2.49*Si + 2.42*Fe + 1.94*Ti + 1.6* (Malm & Hand, 2007). The AERONET values examined include total AOD (AERO) as well as fine mode AOD (FM), coarse mode AOD (CM), 440–870 nm Ångström values (Ång), and the derived FM effective radius (FM r_{eff}).

Scattering and absorption coefficients measured at the ground level closely mirrored the $PM_{2.5}$ correlations between sites, with r^2 ranging from 0.26 to 0.63 (Table 5). As aerosol scattering and absorption coefficients were measured at a dry RH of 13%, 12%, and 13% for CTR, OLF, and YRK, respectively, this reflects the similarity of aerosol mass among the sites, with little variation in the aerosol size distribution and BC aerosol mass. This is in contrast to the variations in dry α_{sp}, which showed very little intersite correlations between the sites (r^2 between 0.0 and 0.33), suggesting that the small variations in α_{sp} are not enough to drive the uncoupling of intersite scattering and absorption coefficients at the surface level and that changes in aerosol mass are the driving factor behind scattering coefficient variability.

Interestingly, the high level of correlation between $PM_{2.5}$ among the four sites is not as strong in the intersite AOD correlation statistics, in either AERONET or satellite. Figure 7a and Table 5 show squared correlation coefficients on intersite AERONET-measured AOD time series (r^2: 0.09–0.51). This suggests that regional atmospheric conditions both at the surface and extending through the vertical that can impact AOD, compounded by instrument errors, vary more than the regional sources and sinks for surface-level aerosols.

4.3. Contribution of RH, Aerosol Chemistry, and Size Distributions to AOD Variability

The above results beg the question how much does knowledge of the aerosol chemistry allow for the prediction of α_{sp} and AOD, and from there better knowledge of the $PM_{2.5}$ mass to AOD relationship. As previous sections have shown that the $PM_{2.5}$-AOD relationship is variable by season and by year, we will return our focus to the data collected during the SEAC^{4}RS campaign, June–September 2013.

As much of the nonlinearity in the $PM_{2.5}$-AOD relationship is due to variability in the vertical, using ground-based extinction measurements should improve the relationship between aerosol mass and aerosol optical properties. Using dry surface-level σ_{sp} instead of AOD in the $PM_{2.5}$ for the linear regressions reveals better association, with r^2 values of 0.90, 0.84, and 0.87 for the CTR, OLF, and YRK sites, respectively. As the σ_{sp} is the product of α_{sp} and $PM_{2.5}$, we can tentatively state that knowledge of the dry aerosol mass extinction efficiency would improve knowledge of surface $PM_{2.5}$ based on AOD measurements at the CTR and YRK sites. Yet no significant linear relationships were found between α_{sp} and either SO_4:OC, OC mass fraction, or SO_4^{2-} mass fraction at the SEARCH sites (Figure 6c; scattering coefficients were not measured at the UAH site). However, the mass of the sulfate and organic carbon were better correlated to α_{sp} than $PM_{2.5}$ mass alone, and summertime α_{sp} tend to peak with sulfate mass concentrations, suggesting some measurable dependency on aerosol chemistry. The r^2 values between OC and α_{sp} were 0.30, 0.36, and 0.15 for CTR, OLF, and YRK. Similarly, they were 0.29, 0.17, and 0.36 between SO_4^{2-} and α_{sp}, and only 0.17, 0.11, and 0.24 between $PM_{2.5}$ mass and α_{sp} at CTR, OLF, and YRK, respectively.

Previous authors have found that α_{sp} is negatively correlated to density, and positively correlated to size (Hand & Malm, 2007), but lack of dry aerosol size distribution measurements make confirmation of this finding impossible for the SEARCH and SEAC^{4}RS campaigns. At 1.77 g/cm^3 ammonium sulfate clearly has a higher density than what is presumed for organics (e.g., $<$1.2 to 1.4 g/cm^3; Turpin & Lim, 2001; Kostenidou et al., 2007). But to explain this difference we would think size would be equally important. However, this is difficult to confirm using the AERONET-derived FM effective radii (Table 3), and there are no long-term AERONET sites where the effective radii can be inferred, except for UAH which begins after 2008. Unlike the dry $PM_{2.5}$ mass and scattering coefficients measured at the SEARCH sites, the FM effective radius is column-averaged, and thus impacted by ambient RH. So if a higher sulfate mass fraction leads to a smaller size distribution at dry RHs and thus a smaller α_{sp}, the greater hygroscopicity of these aerosols would mean they experience more hygroscopic growth at ambient RHs, making differences in size distributions difficult to detect using AERONET derivations.

Another source of complexity in any trends in $PM_{2.5}$-AOD relationships is the impact of aerosol hygroscopic growth, dependent upon both the chemical make-up of the aerosols and the local environmental condition. A large source of variability in the RH is in the vertical with complex mixing of air masses, inconstant PBL heights, and cloud fields. However, there is also observable variability in the horizontal at the surface level. While the average RH was ~80% for the three SEARCH sites, and only 69% at the UAH site, microclimates and variable surface conditions caused variations in the local RHs, resulting in low intersite correlations of RH (Table 5). The best intersite correlation of RH occurred between CTR and YRK, with r^2 at 0.64, and the lowest correlations occurred between OLF and UAH, with an r^2 of only 0.20. These differences, coupled with small

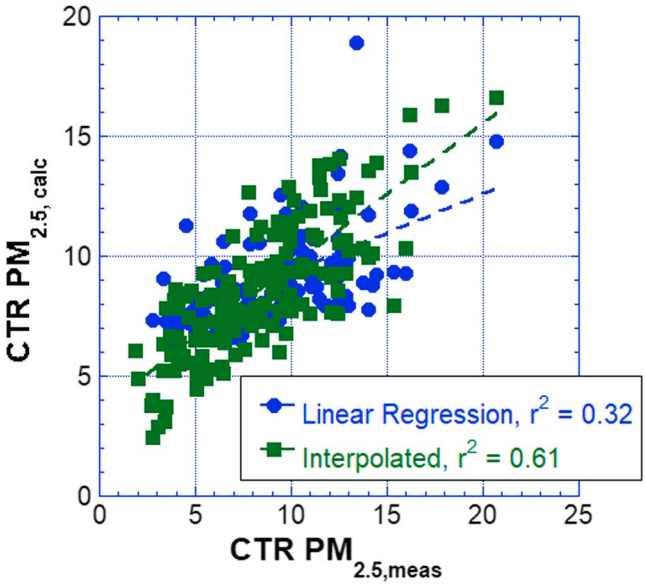

Figure 15. A comparison of predicted $PM_{2.5}$ (μg/m^3) at CTR (CTR $PM_{2.5}$,calc) using the $PM_{2.5}$-AOD linear regression calculation and interpolation using nearby $PM_{2.5}$ observations (CTR $PM_{2.5}$,meas).

differences in the aerosol hygroscopicity, could have a large impact on the column-integrated AODs (e.g., Bian et al., 2009; Brock, Wagner, Anderson, Attwood et al., 2016; Brock, Wagner, Anderson, Beyersdorf et al., 2016; Malm et al., 2005; Wang et al., 2008). Hegg et al. (1997) found that condensed water contributed to, on average, 35% of the total AOD, and as much as 63% off the east coast of the United States. Thus, small variations in local RHs could produce large differences in AODs, even when the dry aerosol mass and chemistry is similar. Unfortunately, direct measurements of aerosol hygroscopicity were not available at the ground sites during the SEAC^{4}RS campaign, so we are unable to quantify the impact of aerosol hygroscopicity on the $PM_{2.5}$-AOD relationship. Using an estimated γ = 0.5 (Lynch et al., 2016) only improved correlation values at the CTR and UAH sites, with resulting $PM_{2.5}$-AOD r^2 of 0.46, 0.31, 0.43, and 0.52 at CTR, OLF, YRK, and UAH, respectively. Using the Attwood et al. (2014) derivation of

$$\gamma = 0.70–0.42\ F_{OA} \tag{8}$$

where F_{OA} is the fraction mass of organic aerosol, we are able to derive a mean daily γ from filter measurements, improving the $PM_{2.5}$-AOD r^2 to 0.51, 0.56, and 0.70 at CTR, OLF, and YRK, respectively. The mean derived γ value used at the three sites were 0.55 ± 0.05, 0.60 ± 0.04, and 0.58 ± 0.02, respectively.

4.4. Using AOD to Predict $PM_{2.5}$

One of the most remarkable results of section 3 is that the $PM_{2.5}$ intersite correlations are significantly better than site-specific AOD-$PM_{2.5}$ correlations, and are also better than the intersite correlations of AOD. To test possible applications of this, we performed interpolation by use of a Delaunay triangulation, which uses circumcircles to interpolate values on a two-dimensional surface (Chew, 1989), on the data collected at the OLF, YRK, and UAH sites to the centrally located CTR site and compared the results to using AERONET AOD measurements and converting them to $PM_{2.5}$ using the linear regression relationships shown in Figure 8. The results are shown in Figure 15, with the $PM_{2.5}$ predicted through interpolation significantly outperforming the $PM_{2.5}$ predicted using the measured AOD and derived linear equation. The r^2 value of 0.61 from the interpolation results suggests that within a similar geographic region, aerosol sources and sinks do not vary as much spatially as the factors controlling the transformation from surface-level $PM_{2.5}$ to column-total AOD. Using the slope and regression from the Theil Sen calculations (Theil, 1950) yielded the same level of correlation as the simple $PM_{2.5}$-AOD linear regression. This suggests krigged $PM_{2.5}$ data set shown in Figures 1a and 1b is more representative of ground-based $PM_{2.5}$ conditions than derivations using the more geographically detailed, but physically complicated AODs shown in Figures 1c and 1d.

5. Final Discussion and Conclusions

$PM_{2.5}$ trends and their relationships to optical observables in the SEUS are complex, and study in this area requires a plethora of data to fully comprehend the geographic and temporal variability. The SEAC^{4}RS summer 2013 field campaigns being the greatest opportunities thus far to provide insight, especially when looked at in the historical context provided by 15 years of ground-based observations performed as part of the SEARCH campaign. During the intensive campaign period the environment experienced relatively stable summertime ridging interspersed by significant convective activity, resulting in changing surface-level $PM_{2.5}$ and AODs. These conditions were further complicated by the addition of transported African dust. This provides a singular opportunity to examine correlations between the variability of $PM_{2.5}$ chemical and optical properties and the resulting AODs. Additionally, the tail end of the SEAC^{4}RS campaign was able to capture the autumnal period with a drop in temperatures accompanied by an increase in frontal activity, presenting a transition in the $PM_{2.5}$ chemistry. We can use the summer 2013 ground network as a baseline for further discussion as to what intensive measurements from aircraft and ground stations really mean, and likewise

provide insight into the monitoring of PM from space. The primary conclusions drawn from our thorough data analysis include the following:

- Intersite correlations of $PM_{2.5}$ are better than AOD intersite correlations. In fact, when using surrounding $PM_{2.5}$ measurements to interpolate $PM_{2.5}$ mass at the CTR site, we found significant improvement over using the site-specific AOD measurements and regression coefficient derived from the $PM_{2.5}$-AOD linear relationship, with coefficient of determination between calculated values and measured values at the CTR site improving from 0.32 to 0.61. Further deterioration of the coefficient of determination is observed when using satellite-derived AODs.
- Multiple nonlinear trends in mass scattering efficiencies were observed, including a decrease with concentration. Additionally, α_{sp} could not be strongly linked to SO_4^{2-}, OC, or a ratio of the two, resisting any easy way of predicting local aerosol optical properties using known major chemical constituents. Thus, linear trends in AOD cannot be expected to be directly translatable to linear trends in $PM_{2.5}$ mass.
- Sulfate and OC are highly correlated and were the primary drivers in $PM_{2.5}$ mass, but their ratio does not appear to relate to other optical properties. The oxidation state of the POM at the SEARCH/SEAC^{4}RS sites falls between a multiplier of 1.4 and 2.4 of OC, within previously observed values.
- Strong seasonal changes occur in both optical properties and vertical distribution, further complicating AOD to $PM_{2.5}$ relationships. This shift in regimes was sudden and observable in drops between the summer and fall season $PM_{2.5}$ mass and accompanying SO_4^{2-} and OC mass, with mean $PM_{2.5}$ mass ranging from 9.7 to 13.4 $\mu g/m^3$ at the four sites in the summer months of 2008–2013 compared to 7.0 to 9.0 $\mu g/m^3$ in the winter months.
- SEAC^{4}RS is representative of the region for the past five years. But significant changes to $PM_{2.5}$ chemistry and mass were observed over the long term. The long-term change in $PM_{2.5}$ mass and chemistry had impacts on the aerosol optical properties. The α_{sp} saw a reduction across all seasons between the 1998–2007 and the 2008–2013 period. This, accompanied by the reduction in aerosol hygroscopicity due to decreasing SO_4^{2-} concentrations, had a clear impact on the $PM_{2.5}$-AOD regression coefficients calculated using satellite-derived AODs, with a steady decline observed in the regression coefficient from 2000 to 2015.
- Thus, while intensive field campaigns are necessary to develop an in-depth understanding of aerosol physical and optical properties at a given location, long-term observation stations are needed to accurately quantify trends that impact the $PM_{2.5}$-AOD relationship.

By providing a thorough examination of different physical, chemical, and optical properties of $PM_{2.5}$ in the SEUS region, we demonstrate the capabilities of the coefficient of determination relationships, and where we are in need of moving beyond, our attempts to optimize this relationship and instead develop new ways of predicting aerosol mass, such as using triangulation methods among existing ground measurements. Our studies suggest that there are large limitations to the use of AOD for prediction of surface-level $PM_{2.5}$ mass. While high-load aerosol events are easily tracked using remote optical observations, more subtle variations in $PM_{2.5}$ are more difficult to predict using only AOD. The $PM_{2.5}$-AOD relationship varies significantly both seasonally and annually due to changes in aerosol mass, chemistry, and resulting optical properties. Our results point to challenges of the use of monitoring air quality via optical means. This is not at all to say that satellite data are without value. Without a doubt air quality monitoring and forecasting systems will continue to improve and make better use of satellite data. This is especially true in data void regions. But the variability between sites in meteorology, and aerosol optical properties, vertical distribution demonstrated studied here naturally points to the large uncertainty developers must cope with. Therefore, the baselining of satellite, modeling, and intensive in situ data sets is still crucial rationale for continued and comprehensive surface monitoring.

Acknowledgments
The SEAC^{4}RS mission required the help and assistance of a number of individuals from all of the participating organizations as listed in the author list. Particular thanks go out to the Environmental Protection Agency for the operation of the CSN network, the Southeastern Aerosol Research and Characterization Network, and NASA and Brent Holben, for the overview and operation of the AERONET network. Funding for the data analysis in this work was provided by a NASA Atmospheric Composition Campaign Data Analysis and Modeling program (NNH14AY68I) and the Office of Naval Research Code 322 (N0001414AF00002). All the data used are listed in the references or archived in the following repositories: http://www.airnowtech.org, https://www3.epa.gov/ttnamti1/speciepg.html, https://aeronet.gsfc.nasa.gov/, and http://views.cira.colostate.edu/fed/DataWizard/Default.aspx.

References

Al-Saadi, J., Szykman, J., Pierce, R. B., Kittaka, C., Neil, D., Chu, D. A., et al. (2005). Improving national air quality forecasts with satellite aerosol observations. *Bulletin of the American Meteorological Society*, *86*(9), 1249–1261.

Alston, E. J., Sokolik, I. N., & Kalashnikova, O. V. (2012). Characterization of atmospheric aerosol in the US Southeast from ground-and space-based measurements over the past decade. *Atmospheric Measurement Techniques*, *5*(7), 1667.

Ångström, A. (1929). On the atmospheric transmission of Sun radiation and on dust in the air. *Geografiska Annaler*, *11*(2), 156–166.

Attwood, A. R., Washenfelder, R. A., Brock, C. A., Hu, W., Baumann, K., Campuzano-Jost, P., et al. (2014). Trends in sulfate and organic aerosol mass in the southeast US: Impact on aerosol optical depth and radiative forcing. *Geophysical Research Letters*, *41*, 7701–7709. https://doi.org/10.1002/2014GL061669

Atwood, S. A., Reid, J. S., Kreidenweis, S. M., Cliff, S. S., Zhao, Y., Lin, N.-H., et al. (2013). Size resolved measurements of springtime aerosol particles over the northern South China Sea. *Atmospheric Environment*, *78*, 134–143.

Bian, H., Chin, M., Rodriguez, J. M., Yu, H., Penner, J. E., & Strahan, S. (2009). Sensitivity of aerosol optical thickness and aerosol direct radiative effect to relative humidity. *Atmospheric Chemistry and Physics*, *9*(7), 2375–2386.

Bond, T. C., Doherty, S. J., Fahey, D. W., Forster, P. M., Berntsen, T., DeAngelo, B. J., et al. (2013). Bounding the role of black carbon in the climate system: A scientific assessment. *Journal of Geophysical Research: Atmospheres*, *118*, 5380–5552. https://doi.org/10.1002/jgrd.50171

Brewer, P., Shepherd, D., Johnson, S., Hand, J. & Schichtel, B. (2014). Implementation of the regional haze rule. *EM Magazine*. Retrieved from http://pubs.awma.org/gsearch/em/2014/5/brewer.pdf, (last accessed 3/15/18).

Brock, C. A., Wagner, N. L., Anderson, B. E., Attwood, A. R., Beyersdorf, A., Campuzano-Jost, P., et al. (2016). Aerosol optical properties in the southeastern United States in summer—Part 1: Hygroscopic growth. *Atmospheric Chemistry and Physics*, *16*(8), 4987–5007.

Brock, C. A., Wagner, N. L., Anderson, B. E., Beyersdorf, A., Campuzano-Jost, P., Day, D. A., et al. (2016). Aerosol optical properties in the southeastern United States in summer—Part 2: Sensitivity of aerosol optical depth to relative humidity and aerosol parameters. *Atmospheric Chemistry and Physics*, *16*(8), 5009–5019.

Brown, J. H., Cook, K. M., Ney, F. G., & Hatch, T. (1950). Influence of particle size upon the retention of particulate matter in the human lung. *American Journal of Public Health and the Nations Health*, *40*(4), 450–480.

Buchard, V., da Silva, A. M., Randles, C. A., Colarco, P., Ferrare, R., Hair, J., et al. (2016). Evaluation of the surface PM 2.5 in version 1 of the NASA MERRA aerosol reanalysis over the United States. *Atmospheric Environment*, *125*, 100–111.

Budisulistiorini, S., Li, X., Bairai, S. T., Renfro, J., Liu, Y., Liu, Y. J., et al. (2015). Examining the effects of anthropogenic emissions on isoprene-derived secondary organic aerosol formation during the 2013 Southern Oxidant and Aerosol Study (SOAS) at the Look Rock, Tennessee ground site. *Atmospheric Chemistry and Physics*, *15*(15), 8871–8888.

Chew, L. P. (1989). Constrained delaunay triangulations. *Algorithmica*, *4*(1–4), 97–108.

Drury, E., Jacob, D. J., Spurr, R. J., Wang, J., Shinozuka, Y., Anderson, B. E., et al. (2010). Synthesis of satellite (MODIS), aircraft (ICARTT), and surface (IMPROVE, EPA-AQS, AERONET) aerosol observations over eastern North America to improve MODIS aerosol retrievals and constrain surface aerosol concentrations and sources. *Journal of Geophysical Research*, *115*, D14204. https://doi.org/10.1029/2009JD012629

Dubovik, O., Smirnov, A., Holben, B. N., King, M. D., Kaufman, Y. J., Eck, T. F., & Slutsker, I. (2000). Accuracy assessments of aerosol optical properties retrieved from Aerosol Robotic Network (AERONET) Sun and sky radiance measurements. *Journal of Geophysical Research*, *105*(D8), 9791–9806.

Edgerton, E. S., Hartsell, B. E., Saylor, R. D., Jansen, J. J., Hansen, D. A., & Hidy, G. M. (2005). The southeastern aerosol research and characterization study: Part II. Filter-based measurements of fine and coarse particulate matter mass and composition. *Journal of the Air & Waste Management Association*, *55*, 1527–1542.

Engel-Cox, J. A., Young, G. S., & Hoff, R. M. (2005). Application of satellite remote-sensing data for source analysis of fine particulate matter transport events. *Journal of the Air & Waste Management Association*, *55*(9), 1389–1397.

Englert, N. (2004). Fine particles and human health—A review of epidemiological studies. *Toxicology Letters*, *149*(1), 235–242.

Ford, B., & Heald, C. L. (2013). Aerosol loading in the southeastern United States: Reconciling surface and satellite observations. *Atmospheric Chemistry and Physics*, *13*(18), 9269–9283.

Gassó, S., Hegg, D. A., Covert, D. S., Collins, D., Noone, K. J., Öström, E., et al. (2000). Influence of humidity on the aerosol scattering coefficient and its effect on the upwelling radiance during ACE-2. *Tellus B*, *52*(2), 546–567.

Gupta, P., Christopher, S. A., Wang, J., Gehrig, R., Lee, Y. C., & Kumar, N. (2006). Satellite remote sensing of particulate matter and air quality assessment over global cities. *Atmospheric Environment*, *40*(30), 5880–5892.

Hand, J. L., Gill, T. E., & Schichtel, B. A. (2017). Spatial and seasonal variability in fine mineral dust and coarse aerosol mass at remote sites across the United States. *Journal of Geophysical Research: Atmospheres*, *122*, 3080–3097. https://doi.org/10.1002/2016JD026290

Hand, J. L., & Malm, W. C. (2007). Review of aerosol mass scattering efficiencies from ground-based measurements since 1990. *Journal of Geophysical Research*, *112*, D16203. https://doi.org/10.1029/2007JD008484

Hand, J. L., Schichtel, B. A., Malm, W. C., Copeland, S., Molenar, J. V., Frank, N., & Pitchford, M. (2014). Widespread reductions in haze across the United States from the early 1990s through 2011. *Atmospheric Environment*, *94*, 671–679.

Hand, J. L., Schichtel, B. A., Malm, W. C., & Frank, N. H. (2013). Spatial and temporal trends in $PM_{2.5}$ organic and elemental carbon across the United States. *Advances in Meteorology*, *2013*, 367674. https://doi.org/10.1155/2013/367674

Hand, J. L., Schichtel, B. A., Pitchford, M., Malm, W. C., & Frank, N. H. (2012). Seasonal composition of remote and urban fine particulate matter in the United States. *Journal of Geophysical Research*, *117*, D05209. https://doi.org/10.1029/2011JD017122

Hansen, D. A., Edgerton, E. S., Hartsell, B. E., Jansen, J. J., Kandasamy, N., Hidy, G. M., & Blanchard, C. L. (2003). The southeastern aerosol research and characterization study: Part 1—Overview. *Journal of the Air & Waste Management Association*, *53*(12), 1460–1471.

Hegg, D. A., Livingston, J., Hobbs, P. V., Novakov, T., & Russell, P. (1997). Chemical apportionment of aerosol column optical depth off the mid-Atlantic coast of the United States. *Journal of Geophysical Research*, *102*(D21), 25,293–25,303.

Hering, S., & Cass, G. (1999). The magnitude of bias in the measurement of PM_{25} arising from volatilization of particulate nitrate from Teflon filters. *Journal of the Air & Waste Management Association*, *49*(6), 725–733.

Hoff, R. M., & Christopher, S. A. (2009). Remote sensing of particulate pollution from space: Have we reached the promised land? *Journal of the Air & Waste Management Association*, *59*(6), 645–675.

Holben, B. N., Eck, T. F., Slutsker, I., Tanre, D., Buis, J. P., Setzer, A., et al. (1998). AERONET—A federated instrument network and data archive for aerosol characterization. *Remote Sensing of Environment*, *66*(1), 1–16.

Hyer, E. J., Reid, J. S., & Zhang, J. (2011). An over-land aerosol optical depth data set for data assimilation by filtering, correction, and aggregation of MODIS Collection 5 optical depth retrievals. *Atmospheric Measurement Techniques*, *4*(3), 379–408.

Kahn, R. A., Gaitley, B. J., Martonchik, J. V., Diner, D. J., Crean, K. A., & Holben, B. (2005). Multiangle Imaging Spectroradiometer (MISR) global aerosol optical depth validation based on 2 years of coincident Aerosol Robotic Network (AERONET) observations. *Journal of Geophysical Research*, *110*, D10S04. https://doi.org/10.1029/2004JD004706

Kahn, R. A., Garay, M. J., Nelson, D. L., Yau, K. K., Bull, M. A., Gaitley, B. J., et al. (2007). Satellite-derived aerosol optical depth over dark water from MISR and MODIS: Comparisons with AERONET and implications for climatological studies. *Journal of Geophysical Research*, *112*, D18205. https://doi.org/10.1029/2006JD008175

Kaku, K. C., Reid, J. S., O'Neill, N. T., Quinn, P. K., Coffman, D. J., & Eck, T. F. (2014). Verification and application of the extended spectral deconvolution algorithm (SDA+) methodology to estimate aerosol fine and coarse mode extinction coefficients in the marine boundary layer. *Atmospheric Measurement Techniques*, *7*(10), 3399–3412.

Kaufman, Y. J., Holben, B. N., Tanré, D., Slutsker, I., Smirnov, A., & Eck, T. F. (2000). Will aerosol measurements from Terra and Aqua polar orbiting satellites represent the daily aerosol abundance and properties? *Geophysical Research Letters*, *27*(23), 3861–3864.

Kerminen, V. M., Teinilä, K., Hillamo, R., & Pakkanen, T. (1998). Substitution of chloride in sea-salt particles by inorganic and organic anions. *Journal of Aerosol Science*, *29*(8), 929–942.

Kostenidou, E., Pathak, R. K., & Pandis, S. N. (2007). An algorithm for the calculation of secondary organic aerosol density combining AMS and SMPS data. *Aerosol Science and Technology*, *41*(11), 1002–1010.

Lary, D. J., Remer, L. A., MacNeill, D., Roscoe, B., & Paradise, S. (2009). Machine learning and bias correction of MODIS aerosol optical depth. *IEEE Geoscience and Remote Sensing Letters*, *6*(4), 694–698.

Levy, R. C., Mattoo, S., Munchak, L. A., Remer, L. A., Sayer, A. M., Patadia, F., & Hsu, N. C. (2013). The Collection 6 MODIS aerosol products over land and ocean. *Atmospheric Measurement Techniques*, *6*, 2989–3034. https://doi.org/10.5194/amt-6-2989-2013

Li, J., Carlson, B. E., & Lacis, A. A. (2015). How well do satellite AOD observations represent the spatial and temporal variability of PM 2.5 concentration for the United States? *Atmospheric Environment*, *102*, 260–273.

Liu, Y., & Daum, P. H. (2000). The effect of refractive index on size distributions and light scattering coefficients derived from optical particle counters. *Journal of Aerosol Science*, *31*(8), 945–957.

Liu, Y., Sarnat, J. A., Kilaru, V., Jacob, D. J., & Koutrakis, P. (2005). Estimating ground-level $PM_{2.5}$ in the eastern United States using satellite remote sensing. *Environmental Science & Technology*, *39*(9), 3269–3278.

Loría-Salazar, S. M., Panorska, A., Arnott, W. P., Barnard, J. C., Boehmler, J. M., & Holmes, H. A. (2017). Toward understanding atmospheric physics impacting the relationship between columnar aerosol optical depth and near-surface PM2. 5 mass concentrations in Nevada and California, USA, during 2013. *Atmospheric Environment*, *171*, 289–300.

Lowenthal, D. H., & Kumar, N. (2004). Variation of mass scattering efficiencies in IMPROVE. *Journal of the Air & Waste Management Association*, *54*(8), 926–934.

Lynch, P., Reid, J. S., Westphal, D. L., Zhang, J., Hogan, T. F., Hyer, E. J., et al. (2016). Development studies towards an 11-year global gridded aerosol optical thickness reanalysis for climate and applied applications. *Geoscientific Model Development*, *9*, 1489–1522. https://doi.org/10.5194/gmd-9-1489-2016

Malm, W. C., Day, D. E., Kreidenweis, S. M., Collett, J. L., Carrico, C., McMeeking, G., & Lee, T. (2005). Hygroscopic properties of an organic-laden aerosol. *Atmospheric Environment*, *39*(27), 4969–4982.

Malm, W. C., & Hand, J. L. (2007). An examination of the physical and optical properties of aerosols collected in the IMPROVE program. *Atmospheric Environment*, *41*(16), 3407–3427.

Malm, W. C., Schichtel, B. A., Hand, J. L., & Collett, J. L. (2017). Concurrent temporal and spatial trends in sulfate and organic mass concentrations measured in the IMPROVE monitoring program. *Journal of Geophysical Research: Atmospheres*, *122*, 10,462–10,476. https://doi.org/10.1002/2017JD026865

Malm, W. C., Schichtel, B. A., & Pitchford, M. L. (2011). Uncertainties in $PM_{2.5}$ gravimetric and speciation measurements and what we can learn from them. *Journal of the Air & Waste Management Association*, *61*(11), 1131–1149.

Malm, W. C., Sisler, J. F., Huffman, D., Eldred, R. A., & Cahill, T. A. (1994). Spatial and seasonal trends in particle concentration and optical extinction in the United States. *Journal of Geophysical Research*, *99*(D1), 1347–1370.

McHenry, J. N., Vukovich, J. M., & Hsu, N. C. (2015). Development and implementation of a remote-sensing and in situ data-assimilating version of CMAQ for operational PM2. 5 forecasting. Part 1: MODIS aerosol optical depth (AOD) data-assimilation design and testing. *Journal of the Air & Waste Management Association*, *65*(12), 1395–1412.

Nguyen, T. K. V., Ghate, V. P., & Carlton, A. G. (2016). Reconciling satellite aerosol optical thickness and surface fine particle mass through aerosol liquid water. *Geophysical Research Letters*, *43*, 11,903–11,912. https://doi.org/10.1002/2016GL070994

O'Neill, N. T., Eck, T. F., Smirnov, A., Holben, B. N., & Thulasiraman, S. (2003). Spectral discrimination of coarse and fine mode optical depth. *Journal of Geophysical Research*, *108*(D17), 4559. https://doi.org/10.1029/2002JD002975

Petrenko, M., Ichoku, C., & Leptoukh, G. (2012). Multi-sensor Aerosol Products Sampling System (MAPSS). *Atmospheric Measurement Techniques*, *5*, 913–926. https://doi.org/10.5194/amt-5-913-2012

Quinn, P. K., & Coffman, D. J. (1998). Local closure during the First Aerosol Characterization Experiment (ACE 1): Aerosol mass concentration and scattering and backscattering coefficients. *Journal of Geophysical Research*, *103*(D13), 16,575–16,596. https://doi.org/10.1029/97JD03757

Reid, J. S., Hobbs, P. V., Liousse, C., Martins, J. V., Weiss, R. E., & Eck, T. F. (1998). Comparisons of techniques for measuring shortwave absorption and black carbon content of aerosols from biomass burning in Brazil. *Journal of Geophysical Research*, *103*(D24), 32,031–32,040.

Reid, J. S., Kuehn, R. E., Holz, R. E., Eloranta, E. W., Kaku, K. C., Kuang, S., et al. (2017). Ground-based high spectral resolution lidar observation of aerosol vertical distribution in the summertime southeast United States. *Journal of Geophysical Research: Atmospheres*, *122*, 2970–3004. https://doi.org/10.1002/2016JD025798

Ross, J. L., Hobbs, P. V., & Holben, B. (1998). Radiative characteristics of regional hazes dominated by smoke from biomass burning in Brazil: Closure tests and direct radiative forcing. *Journal of Geophysical Research*, *103*(D24), 31,925–31,941. https://doi.org/10.1029/97JD03677

Roy, B., Mathur, R., Gilliland, A. B., & Howard, S. C. (2007). A comparison of CMAQ-based aerosol properties with IMPROVE, MODIS, and AERONET data. *Journal of Geophysical Research*, *112*, D14301. https://doi.org/10.1029/2006JD008085

Rubin, J. I., Reid, J. S., Hansen, J. A., Anderson, J. L., Holben, B. N., Xian, P., et al. (2017). Assimilation of AERONET and MODIS AOT observations using variational and ensemble data assimilation methods and its impact on aerosol forecasting skill. *Journal of Geophysical Research: Atmospheres*, *122*, 4967–4992. https://doi.org/10.1002/2016JD026067

Schichtel, B. A., Hand, J. L., Barna, M. G., Gebhart, K. A., Copeland, S., Vimont, J., & Malm, W. C. (2017). Origin of fine particulate carbon in the rural United States. *Environmental Science & Technology*, *51*(17), 9846–9855.

Schmid, B., Livingston, J. M., Russell, P. B., Durkee, P. A., Jonsson, H. H., Collins, D. R., et al. (2000). Clear-sky closure studies of lower tropospheric aerosol and water vapor during ACE-2 using airborne sunphotometer, airborne in-situ, space-borne, and ground-based measurements. *Tellus Series B: Chemical and Physical Meteorology*, *52*(2), 568–593.

Schwartz, C. S., Liu, Z., Lin, H. C., & McKeen, S. A. (2012). Simultaneous three-dimensional variational assimilation of surface fine particulate matter and MODIS aerosol optical depth. *Journal of Geophysical Research*, *117*, D13202. https://doi.org/10.1029/2011JD017383

Sessions, W. R., Reid, J. S., Benedetti, A., Colarco, P. R., da Silva, A., Lu, S., et al. (2015). Development towards a global operational aerosol consensus: Basic climatological characteristics of the International Cooperative for Aerosol Prediction Multi-Model Ensemble (ICAP-MME). *Atmospheric Chemistry and Physics Discussions*, *14*(10), 14,933–14,998.

Shi, Y., Zhang, J., Reid, J. S., Holben, B., Hyer, E. J., & Curtis, C. (2011). An analysis of the collection 5 MODIS over-ocean aerosol optical depth product for its implication in aerosol assimilation. *Atmospheric Chemistry and Physics*, *11*, 557–565. https://doi.org/10.5194/acp-11-557-2011

Shinozuka, Y., Clarke, A. D., Nenes, A., Jefferson, A., Wood, R., McNaughton, C. S., et al. (2015). The relationship between cloud condensation nuclei (CCN) concentration and light extinction of dried particles: Indications of underlying aerosol processes and implications for satellite-based CCN estimates. *Atmospheric Chemistry and Physics*, *15*(13), 7585–7604. https://doi.org/10.5194/acp-15-7585-2015

Smirnov, A., Holben, B. N., Eck, T. F., Dubovik, O., & Slutsker, I. (2000). Cloud-screening and quality control algorithms for the AERONET database. *Remote Sensing of Environment*, *73*(3), 337–349.

Theil, H. (1950). A rank-invariant method of linear and polynomial regression analysis. *Proceedings of the Koninklijke Nederlandse Akademie van Wetenschappen A*, *53*(386–392.521-525), 1397–1412.

Toon, O. B., Maring, H., Dibb, J., Ferrare, R., Jacob, D. J., Jensen, E. J., et al. (2016). Planning, implementation, and scientific goals of the Studies of Emissions and Atmospheric Composition, Clouds and Climate Coupling by Regional Surveys (SEAC4RS) field mission. *Journal of Geophysical Research: Atmospheres*, *121*, 4967–5009. https://doi.org/10.1002/2015JD024297

Tosca, M. G., Campbell, J., Garay, M., Lolli, S., Seidel, F. C., Marquis, J., & Kalashnikova, O. (2017). Attributing accelerated summertime warming in the southeast united states to recent reductions in aerosol burden: Indications from vertically-resolved observations. *Remote Sensing*, *9*(7), 674.

Toth, T. D., Zhang, J., Campbell, J. R., Hyer, E. J., Reid, J. S., Shi, Y., & Westphal, D. L. (2014). Impact of data quality and surface-to-column representativeness on the PM 2.5/satellite AOD relationship for the contiguous United States. *Atmospheric Chemistry and Physics*, *14*(12), 6049–6062. https://doi.org/10.5194/acp-14-6049-2014

Turpin, B. J., & Lim, H. J. (2001). Species contributions to $PM_{2.5}$ mass concentrations: Revisiting common assumptions for estimating organic mass. *Aerosol Science & Technology*, *35*(1), 602–610.

U.S. Environmental Protection Agency (2004). "PM2.5 speciation network newsletter," Vol. 1, no. 1. Retrieved from http://www.epa.gov/ttn/amtic/files/ambient/pm25/spec/spnews1.pdf, (last accessed 3/15/18).

Van Donkelaar, A., Martin, R. V., Brauer, M., Kahn, R., Levy, R., Verduzco, C., & Villeneuve, P. J. (2010). Global estimates of ambient fine particulate matter concentrations from satellite-based aerosol optical depth: Development and application. *Environmental Health Perspectives*, *118*(6), 847.

Wagner, N. L., Brock, C. A., Angevine, W. M., Beyersdorf, A., Campuzano-Jost, P., Day, D., et al. (2015). In situ vertical profiles of aerosol extinction, mass, and composition over the southeast United States during SENEX and $SEAC^4RS$: Observations of a modest aerosol enhancement aloft. *Atmospheric Chemistry and Physics*, *15*(12), 7085–7102.

Wang, J., & Christopher, S. A. (2003). Intercomparison between satellite-derived aerosol optical thickness and $PM_{2.5}$ mass: Implications for air quality studies. *Geophysical Research Letters*, *30*(21), 2095. https://doi.org/10.1029/2003GL018174

Wang, J., Jacob, D. J., & Martin, S. T. (2008). Sensitivity of sulfate direct climate forcing to the hysteresis of particle phase transitions. *Journal of Geophysical Research*, *113*, D11207. https://doi.org/10.1029/2003GL018174

Weber, R. J., Sullivan, A. P., Peltier, R. E., Russell, A., Yan, B., Zheng, M., et al. (2007). A study of secondary organic aerosol formation in the anthropogenic-influenced southeastern United States. *Journal of Geophysical Research*, *112*, D13302. https://doi.org/10.1029/2007JD008408

White, W. H., Trzepla, K., Hyslop, N. P., & Schichtel, B. A. (2016). A critical review of filter transmittance measurements for aerosol light absorption, and de novo calibration for a decade of monitoring on PTFE membranes. *Aerosol Science and Technology*, *50*(9), 984–1002.

Xian, P., Kuciauskas, A. P., Reid, J. S. & Zhang, J. (2016). Characterization of Saharan air layer with a combination of decade-long aerosol reanalysis, satellite products and in situ observations. In *AGU Fall Meeting Abstracts*.

Yu, C., Chen, L., Su, L., Fan, M. & Li, S. (2011). Kriging interpolation method and its application in retrieval of MODIS aerosol optical depth. *Geoinformatics, 2011 19th International Conference* (pp. 1–6). IEEE.

Yu, X. Y., Lee, T., Ayres, B., Kreidenweis, S. M., Malm, W., & Collett, J. L. (2006). Loss of fine particle ammonium from denuded nylon filters. *Atmospheric Environment*, *40*(25), 4797–4807.

Zhang, J., & Reid, J. S. (2006). MODIS aerosol product analysis for data assimilation: Assessment of over-ocean level 2 aerosol optical thickness retrievals. *Journal of Geophysical Research*, *111*, D22207. https://doi.org/10.1029/2005JD006898

Zhang, J., Reid, J. S., Westphal, D. L., Baker, N. L., & Hyer, E. J. (2008). A system for operational aerosol optical depth data assimilation over global oceans. *Journal of Geophysical Research*, *113*, D10208. https://doi.org/10.1029/2007JD009065

Zheng, M., Cass, G. R., Schauer, J. J., & Edgerton, E. S. (2002). Source apportionment of $PM_{2.5}$ in the southeastern United States using solvent-extractable organic compounds as tracers. *Environmental Science & Technology*, *36*(11), 2361–2371.

Ziemba, L. D., Lee Thornhill, K., Ferrare, R., Barrick, J., Beyersdorf, A. J., Chen, G., et al. (2013). Airborne observations of aerosol extinction by in situ and remote-sensing techniques: Evaluation of particle hygroscopicity. *Geophysical Research Letters*, *40*, 417–422. https://doi.org/10.1029/2012GL054428